Kent Academic Repository

Full text document (pdf)

Citation for published version

Stephens, Nicholas B and Kivell, Tracy L. and Pahr, Dieter H and Hublin, Jean-Jacques and Skinner, Matthew M. (2018) Trabecular bone patterning across the human hand. Journal of Human Evolution . ISSN 0047-2484.

DOI

https://doi.org/10.1016/j.jhevol.2018.05.004

Link to record in KAR

http://kar.kent.ac.uk/67213/

Document Version

Author's Accepted Manuscript

Accepted in May 2018 at the *Journal of Human Evolution*

Trabecular bone patterning across the human hand

Nicholas B. Stephens [a,*], Tracy L. Kivell [b, a], Dieter H. Pahr [c], Jean-Jacques Hublin [a], Matthew M. Skinner [b, a]

[a] *Department of Human Evolution, Max Planck Institute for Evolutionary Anthropology, Deutscher Platz 6, 04103 Leipzig, Germany*

[b] *Skeletal Biology Research Centre, School of Anthropology and Conservation, University of Kent, Canterbury CT2 7NZ, United Kingdom*

[c] Institute for Lightweight Design and Structural Biomechanics, Vienna University of Technology, Getreidemarkt 9, A-1060 Vienna, Austria

[*] Corresponding author

E-mail address: nick_stephens@eva.mpg.de (N. B. Stephens)

Keywords: Hand evolution; Trabecular bone; Functional morphology; Biomechanics; Behavioral reconstruction; Histomorphometry

Abstract

Hand bone morphology is regularly used to link particular hominin species with behaviors relevant to cognitive/technological progress. Debates about the functional significance of differing hominin hand bone morphologies tend to rely on establishing phylogenetic relationships and/or inferring behavior from epigenetic variation arising from mechanical loading and adaptive bone modeling. Most research focuses on variation in cortical bone structure, but additional information about hand function may be provided through the analysis of internal trabecular structure. While primate hand bone trabecular structure is known to vary in ways that are consistent with expected joint loading differences during manipulation and locomotion, no study exists that has documented this variation across the numerous bones of the hand. We quantify the trabecular structure in 22 bones of the human hand (early/extant modern *Homo sapiens*) and compare structural variation between two groups associated with post-agricultural/industrial (post-Neolithic) and foraging/hunter-gatherer (forager) subsistence strategies. We (1) establish trabecular bone volume fraction (BV/TV), modulus (E), degree of anisotropy (DA), mean trabecular thickness (Tb.Th) and spacing (Tb.Sp); (2) visualize the average distribution of site-specific BV/TV for each bone; and (3) examine if the variation in trabecular structure is consistent with expected joint loading differences among the regions of the hand and between the groups. Results indicate similar distributions of trabecular bone in both groups, with those of the forager sample presenting higher BV/TV, E, and lower DA, suggesting greater and more variable loading during manipulation. We find indications of higher loading along the ulnar side of the forager sample hand, with high site-specific BV/TV distributions among the carpals that are suggestive of high loading while the wrist moves through the ‘dart-thrower’s’ motion. These results support the use of trabecular structure to infer behavior and have direct implications for refining our understanding of human hand evolution and fossil hominin hand use.

Introduction

Interest in primate hand morphology and function is longstanding (e.g., Jones, 1916; Ashley-Montagu, 1931; Napier, 1960; Lewis, 1969; Susman, 1979; Diogo et al., 2012; Boyer et al., 2013), as the hand interacts with substrates during locomotion (e.g., Doran, 1993; Daver et al., 2012; Congdon and Ravosa, 2016) while also facilitating dexterous manipulation during social grooming (Whiten et al., 1999; Brand et al., 2017), food acquisition (Hunt, 1991; Boesch and Boesch, 1993; Visalberghi et al., 2009), communication (Hopkins et al., 2005; Zlatev, 2008), and complex object manipulations (Marzke and Wullstein, 1996; Viaro et al., 2017). Among primates, humans are often cited as the most dexterous (Napier, 1960; Vereecke and Wunderlich, 2016), possessing a suite of morphological features that allow for a wide range of wrist movements, power 'squeeze' grips (Marzke et al., 1992), and the formation of stable precision grips via the forceful opposition of the thumb and finger-pads (Napier, 1956; Marzke 1997; Susman, 1998). Early interpretations favored a view that human dexterity was derived, with researchers drawing strong causal links with hominin bipedal locomotion, the emergence of stone tool use, and/or increased carnivory (Young, 2003; Wood, 2014; Lemelin and Schmitt, 2016). Although most researchers still agree that the distinct aspects of human hand morphology are related to the selective pressures of at least three million years of tool-related behaviors (e.g., Napier, 1956; Washburn, 1960; Marzke, 1997; Harmand et al., 2015), there is less certainty about which features reflect a conserved ancestral state and which are derived (Tocheri et al., 2008; Rolian et al., 2010). This shift in our evolutionary understanding is the direct result of improved comparative techniques (Boyer et al., 2013; Almécija et al., 2015a; Boyer et al., 2015), new fossil discoveries (Kivell et al., 2011a, 2015; Lorenzo et al., 1999, 2015;

Almécija et al., 2012) and more comprehensive observational studies of non-human primate hand use (Hopkins et al., 2011; Marzke et al., 2015; Proffitt et al., 2016; Neufuss et al., 2017), which suggest that human-like hand morphology and use is more generalized and deep-rooted than previously appreciated (Alba et al., 2003; Almécija et al., 2010; Almécija and Alba, 2014; Rolian, 2016).

Thus, a greater understanding of how hand function may be reflected in hand morphology is needed. Variation in hand morphology has been key to informing hypotheses about not only manipulative behaviors and technological abilities in the human past (Leakey et al., 1964; Musgrave, 1971; Vlček, 1975; Susman, 1991, 1994; Niewoehner et al., 2003; Eren and Lycett, 2012; Wood, 2014), but also locomotor habits (Ricklan, 1987; Alba et al., 2003; Shrewsbury et al., 2003; Green and Gordon, 2008; Kivell, 2016), and—more indirectly—human neurological evolution and language acquisition (e.g., Falk, 1980; Hopkins, 2013; Putt et al., 2017). Interpreting hand function in the past is further complicated by the tendency for hominin fossil hand-remains to be recovered in isolation or as unassociated collections (Bush et al., 1982; Schmid and Berger, 1997; Venkataraman et al., 2013; Ward et al., 2014; Domínguez-Rodrigo et al., 2015; Lorenzo et al., 2015; Stratford et al., 2016; Daver et al., in press). As such, it is useful to explore methods with the potential to provide additional functional information about how manual behavior may have varied in the past that can also be applied to isolated hand bone elements.

Bone functional adaptation

Traditionally, researchers have compared the external shape of fossil hominin hand bones to generate hypotheses about hand function and grip capacity. For example, the potential for forming the precision and power grips observed during tool manufacture/use tend to be inferred from the hand proportions (i.e., thumb length relative to finger length) and shape of the trapezium-first metacarpal joint (e.g., Napier, 1962; Trinkaus, 1989; Godinot and Beard, 1991; Susman, 1994; Alba et al., 2003; Tocheri et al., 2003; Marzke et al., 2010). These morphological associations are established through observational studies focusing on wild and captive primate manipulative habits (e.g., Pouydebat et al., 2009, 2011, 2014; Bardo et al., 2015, 2016; Marzke et al., 2015; Orr, 2017), which provide the basis for understanding if extinct taxa with similar morphologies had similar manipulative capacities (e.g., Almécija et al., 2010; Almécija and Alba, 2014; Kivell et al., 2015; Orr, 2018). However, as external morphology only allows inferences about manipulative capacity, and not necessarily actual behavior, many researchers have begun to quantify epigenetic changes to bone that result from repetitive loading (e.g., compression, tension, and shear; Frost, 1987).

This phenomenon, commonly referred to as bone functional adaptation, has been experimentally observed to alter the structure in ways that improve the mechanical competence of repeatedly-loaded bone (Lanyon and Rubin, 1985; Pontzer et al., 2006; Ruff et al., 2006; Barak et al., 2011; Schulte et al., 2013; Christen et al., 2014; Cresswell et al., 2016; Christen and Muller, 2017; Ritter et al., 2017). For instance, cortical bone adjusts in thickness for improved resistance to bending forces, while trabecular bone alters the thickness, spacing, and orientation of struts adjacent to loaded regions in a way that enhances the transfer of kinetic energy away from joint surfaces (Cowin et al., 1985; Keaveny et al., 2001; Sugiyama et al., 2010; Currey, 2011; Barak et al., 2013; Reznikov et al., 2015; but see Demes et al., 1998; Ozcivici and Judex, 2014; Wallace et al., 2015a, b; Fairfield et al., 2017). In general, many regions of the primate skeleton exhibit evidence of adaptive modeling, with structural variation aligning with hypothesized loading differences (e.g., Rafferty and Ruff, 1994; Ryan and Ketcham, 2002; Stock, 2006; Marchi and Shaw, 2011; Ryan and Shaw, 2012; Su et al., 2013; Chirchir, 2015; Fabre et al., 2017; Reznikov et al., 2017; Stieglitz et al., 2017), and hand bone variation reflecting known locomotor, postural, and manipulatory habits (e.g., Marchi, 2005; Patel and Carlson, 2007; Lazenby et al., 2008a, b,2011a; Zeininger et al., 2011; Tsegai et al., 2013; Barak et al., 2017; Chirchir et al., 2017b).

For hand trabecular bone, there are some studies that have reported ambiguous results between inferred loading and structure (e.g., Lazenby et al., 2011a; Schilling et al., 2014; Stephens et al., 2016a; Reina et al., 2017), with overlapping or unanticipated levels of bone volume fraction (BV/TV) and trabecular strut alignment (degree of anisotropy; DA). Explanations for such inconsistencies are found in well-controlled experiments, which utilize animal models to highlight how bone modeling may be influenced by genetic, systemic, or hormonal variation (e.g., Wallace et al., 2010, 2015a; Schlecht et al., 2014; Smith et al., 2014; Fairfield et al., 2017; see Wallace et al., 2017b for a recent review). Among humans, these factors are best understood as they relate to bone’s role in maintaining homeostasis, with differences in bone structure arising from nutritional stress (e.g., anemia, pregnancy) or advanced age (e.g., menopause, osteoporosis; Agarwal, 2016). For trabecular bone these changes are documented in modern and archaeological contexts, with shifts from high BV/TV and low DA (more isotropic) to relatively low BV/TV and high DA (more anisotropic), which prioritizes resistance to load along a singular axis (Singh et al., 1970; Agarwal et al., 2004; Christen et al., 2014; Beauchesne et al., 2017). Much of this understanding has come from the ability to perform more comprehensive quantitative analyses, which better characterize local micro-structural changes in bone (Poole et al., 2012; Gee and Treece, 2014; Gross et al., 2014; Hermann and Klein, 2015; Phillips et al., 2015). This is especially evident in trabecular studies, which have moved from single volume of interest (VOI) analyses to the simultaneous analyses of multiple VOIs (Su and Carlson, 2017; Sylvester et al., 2017) or the whole-bone/epiphysis (Gross et al., 2014; Taghizadeh et al., 2017).

For hand bones, such methods have documented differences in the distribution of trabeculae in the primate third metacarpal (Mc3) that align with predicted joint loading during locomotion and manipulation (Tsegai et al., 2013; Chirchir et al., 2017b; Barak et al., 2017). Other studies have identified similar distributions of BV/TV in human and fossil hominin metacarpals, which suggests a shared pattern of joint loading that may be related to opposition on the thumb during the use of precision grips (Skinner et al., 2015a, b; Stephens et al., 2016a; but see Almécija et al., 2015b). Such results establish the value of trabecular bone analysis to examine aspects of extant and fossil primate manual behavior, which we explore here through the quantification of trabeculae from the articulated elements of the wrist, metacarpus, and phalanges of human (*Homo sapiens*) hands (excluding the pisiform and distal phalanges).

To assess if trabecular architecture of the hand is related to differences in manipulatory loading, we follow previous analyses of other skeletal regions (e.g., Ryan and Shaw, 2015; Scherf et al., 2016; Stieglitz et al., 2017), and compare two groups of humans broadly defined by subsistence strategy and assumed behavior (i.e., community dwelling post-Neolithic agriculturalists/industrialists and mixed foraging/hunter-gatherers; hereafter ‘post-Neolithic’ and ‘forager’, respectively). While these categories are reductionist given the temporogeographically disparate sample (see methods), our aim here is to establish a generalized view of trabecular distribution among the interrelated regions of the human hand. If there are morphological differences attributable to variation in manipulative loading, then these results should be useful in examining more refined questions about individual or group differences in hand use (e.g., between males and females or across occupations; Macintosh et al., 2014, 2017; Sládek 2016; Karakostis 2017), or joined with studies utilizing cortical mapping and/or geometric morphometric techniques to address questions about skeletal variation in complete, incomplete, or unassociated fossil hand remains (e.g., Ward et al., 2014; Domínguez-Rodrigo et al., 2015; Lorenzo et al., 2015; Stratford et al., 2016). Predictions for how human hand trabecular structure may vary follow after a brief review of human hand and wrist kinematics.

Although the interactions at the base of the metacarpals are complex, a simplified understanding may be reached by dividing the hand into radial, ulnar, and thumb portions, according to their movement. The radial portion is rendered relatively immobile by a tight binding of ligaments at the Mc2–Mc3 bases and CMC joint congruence (predominantly the trapezoid and capitate; Brand and Hollister, 1993; Lazenby et al., 2008b; Tocheri et al., 2008). The Mc4–Mc5 in the ulnar portion, however, share a complimentary articular surface with the hamate, which allows these bones to rotate and translate as they flex up to 15 and 30º, respectively (El-Shennawy et al., 2001; Lazenby et al., 2008a; Halilaj et al., 2014; Drapeau, 2015). Thumb opposition is a complex movement facilitated by the saddle-shaped TMC articulation. Specifically, opposition of the thumb causes the Mc1 base to abduct, flex, rotate, and translate ulnarly across the trapezial surface (Halilaj et al., 2015), while the thenar musculature appears to prevent dislocation under load by locking it in place (Brand and Hollister, 1993; D'Agostino et al., 2017).

Potential loading differences

As with previous research, here we assume that variation in trabecular structure between the post-Neolithic and forager samples will be related to differences in activity levels (Polk, 2002; Rhodes and Knusel, 2005; Barak et al., 2011; Shaw et al., 2012; Rabey et al., 2015; Stieglitz et al., 2017; Wallace et al., 2017b). Similar inferences have been drawn in relation to skeletal variation within the lower and upper body, with highly mobile groups demonstrating a generally more robust skeletal structure as a result of repeated and higher loading than more recent humans (Trinkaus et al., 1994; Stock, 2006; Chirchir et al., 2015, 2017a; Ryan and Shaw 2015; Friedl et al., 2016; Scherf et al., 2016). The external morphology of *H. sapiens* hand bones has remained fairly stable from ~100 ka onward, with a notable reduction in morphological features associated with intense, repetitive loading being explained by humans shifting to more mechanically-advantaged technologies (e.g., TMC/Mc5 base; Niewoehner, 2001, 2006; Trinkaus, 2016). In this vein, Stock et al. (2013) reported low levels of right-side bias in the hunter-gatherer Mc2 cortical bone thickness (62.5%), relative to that of the humerus (83.6%), which contrasted with the fairly consistent right-side bias for both skeletal elements in the medieval and industrial samples. This result suggests more equally dispersed bimanual loading for the hunter-gatherer sample, which is consistent with hand use experiments documenting high loading in the dominant or non-dominant hand during various subsistence activities (e.g., butchering, percussive activities; Rolian et al., 2011; Shaw et al., 2012; Key and Dunmore 2015; Key, 2016; Key et al., 2017; Williams-Hatala et al., 2017).

Following from this, variations in hand loading will most likely be related to grips and hand postures that invoke different levels of loading. For instance, less strenuous precision tasks tend to involve the pads of the fingers and only the dominant hand (e.g., low force, tip-to-tip pinch), while more strenuous tasks tend to involve stable grips (e.g., high force, key-grips and/or power grips) utilizing one or both hands (Marzke et al., 1998; Bullock et al., 2010; Williams et al., 2010; Key and Lycett, 2011, 2016; Borel et al., 2016). From these grips the muscle co-contraction and joint reaction forces are uniformly displaced into the radius and ulna during manipulation, with the radial side of the hand displacing most of the force (Gislason et al., 2009, 2010; Pataky et al., 2012; Chen et al., 2014; Márquez-Florez et al., 2015). Even so, high loading is present even during banal manipulations (e.g., pinch force during pipetting; Wu et al., 2015) and—given the physiological limits to modeling (Lambers et al., 2013; Cresswell et al., 2016; Yang et al., 2017)—this may result in generally similar trabecular parameters in the bones along the radial side of the hand (e.g., phalanges, Mc1, Mc2, trapezium, trapezoid). Instead, differences in loading may be more evident along the ulnar side of the hand, where kinetic energy is dissipated during strenuous manual activities that invoke the use of a power grip and involve wrist movements typified by the ‘dart-thrower’s’ motion (e.g., throwing or hammering; Iwasaki et al., 1998; Young, 2003; Majima et al., 2008; Varga et al., 2013; Gabra and Li, 2016; Liu et al., 2016b; Rainbow et al., 2016). Aside from this, subtle differences in the distribution of site-specific BV/TV may be discernable in various anatomical regions, with higher values indicating areas of localized modeling from frequent joint loading.

Predictions

Given the overall (presumed) similarity in hard and soft tissue morphology across all *H. sapiens*, we predict that the pattern of loading interpreted from the trabecular structure will be broadly similar between the two groups, i.e., (1) reflecting flexion at the interphalangeal joints; (2) flexion and adduction/abduction at the metacarpophalangeal joints; and (3) similar patterns of movement and loading at the TMC and intercarpal joints. However, previous research suggests that the trabecular structure of the hand in the forager sample should be consistent with greater levels of loading in the upper body and more variable hand use when compared to the post-Neolithic sample. Thus, we predict that (4) foragers will have on average higher BV/TV and elastic modulus (E) than the post-Neolithic sample, but lower DA due to more varied loading of the hand. Finally, we predict that (5) these differences in hand use will be reflected in how the trabeculae are distributed—e.g., higher site-specific BV/TV in functionally relevant locations, such as palmoulnar concentrations in the Mc2–Mc5 heads (Skinner et al., 2015a, b) and the palmoradial region of the Mc1 (Stephens et al., 2016a).

Materials and methods

Skeletal sample

Table 1 shows all manual skeletal elements of post-Neolithic and forager *H. sapiens* analyzed in this study. While sample sizes for some bones are small, this reflects the paucity of archaeological/paleontological remains with (relatively) complete hands available for microtomographic (μCT) scanning. The post-Neolithic sample is composed of 26 individuals, including associated hand skeletons of 10 Nubian Egyptians (6th–11th century; Strouhal and Jungwirth, 1979; Paoli et al., 1993), 10 individuals from a cemetery in Inden, Germany (18th–19th century), four from Medieval Canterbury, UK (11th–15th century; Hicks et al., 2001), and two from Syracuse, Sicily (20th century). The forager sample is composed of 16 individuals, including associated and isolated remains of eight individuals from Tiera del Fuego (19th century; Marangoni et al., 2011), eight individuals from Věstonice/Pavlov (~23 ka; Sládek, 2000), Arene Candide 2 (9900–10,850 uncal BP; Sparacello et al., 2015), one individual from Lapa do Santo, Brazil (~9.2 ka; Strauss et al., 2015), Barma Grande 2 (~24 Ka; Formicola et al., 1990; Churchill and Formicola, 1997), Ohalo II (~19 ka; Hershkovitz et al., 1995), and Qafzeh 8 and 9 (~80–130 ka; Schwarcz et al., 1988).

As pointed out by Friedl et al. (2016), the grouping of individuals from such a broad temporal range certainly obscures some subtle osteological differences, which should be kept in mind here. Still, a recent study of long-bone cross-sectional geometry likens the upper-limb activity patterns/levels of early *H. sapiens* (e.g., Qafzeh, Ohalo 2, and Gravettian) to contemporary forager samples (e.g., Khoesan), as opposed to Neanderthals (Pearson and Sparacello, 2017), which suggests that the manual loading among the forager sample would be similar enough for the main purposes of this analysis. Similarly, while some variation in manual loading and bone modeling may be related to sex and the sexual division of labor (e.g., Agarwal

2016; Macintosh 2014, 2017; but see Chirchir et al., 2017a), there are also issues with confidently attributing sex to early modern *H. sapiens* based on morphology alone (Mittnik et. al., 2016). Here the pooled sample is used to establish a general overview of trabecular variation that may then be subdivided into samples where there is higher confidence in the age, sex, occupation, and cultural affinity of the individuals.

MicroCT scanning

Microtomographic scans of the samples were obtained using either a SkyScan 1173 at 100–130 kV and 90–130 µA, a SkyScan 1176 scanner at 70 kV and 278 µA, a BIR ACTIS 225/300 scanner at 130 kV and 100–120 µA, or a Diondo d3 at 100–140 kV and 100–140 µA at an average isotopic voxel size of ~29 µm (range = 24–38 µm). Scans were reconstructed as 16-bit TIFF stacks, and each bone was isolated and reoriented to its approximate anatomical position in Avizo® 9.0 (FEI Visualization Sciences Group, Hillsboro, USA). During this process, the internal microstructure was visually assessed on a slice-by-slice basis and pathological or heavily damaged skeletal elements were removed from the sample. In the event that heavy sedimentation was present, manual removal was performed using a Wacom board (Coleman, 2003) and the Avizo paint-brush tool in the labels-field. In instances where the contrast between bone and sediment was impossible to distinguish, the entire section (e.g., the head or base of a metacarpal) was excluded from analyses (see Supplementary Online Material [SOM] Table S1).

Trabecular bone quantification and characterization

The methods employed in this study are described in detail elsewhere and are only briefly summarized here. An illustration of the workflow, along with the specific software packages, may be found in the SOM S1. In short, each bone was segmented using the Ray Casting Algorithm (Scherf and Tilgner, 2009) and then the script-based whole bone/epiphyseal approach Medtool v4.0 (Dr. Pahr Ingenieurs e.U, 2017; see below) was used to extract the cortical bone from the trabecular bone and generate a fine tetrahedral mesh representing the morphology of both tissues (Gross et al., 2014). Quantification of BV/TV, E, and DA of the trabecular mesh was performed in 3D by moving a 5 mm spherical VOI along a background grid with 2.5 mm spacing for each scan (Pahr and Zysset, 2009b), while mean trabecular thickness (Tb.Th, mm) and mean trabecular spacing (Tb.Sp, mm) were calculated following Hildebrand and Ruegsegger (1997). For further details see SOM S1 and SOM Figure. S1.

BV/TV is expressed as a percentage (bone voxels/total voxels), while DA is scaled between 1-0 (anisotropic-isotropic). We focus our analyses on these measures because previous studies show that they are not correlated with body mass (Doube et al., 2011; Barak et al., 2013; Ryan and Shaw, 2013) and are informative in regards to fracture resistance and relative arrangement (Maquer et al., 2015; Pahr and Zysset, 2009a, 2016). E is estimated using a reference tissue of $E_0 = 10$ GPa; $v_0 = 0.3$; $\mu_0 = 3$ GPa based on the Zysset-Curnier model (Zysset, 2003), which produces a more accurate measure by accounting for both BV/TV and fabric (Haïat et al., 2009; Latypova et al., 2017). This parameter identifies a material's mechanical ability to resist deformation under load (Zysset, 2003; Currey, 2011).

We compare these parameters for the whole carpal (capitate, hamate, lunate, scaphoid, trapezoid, trapezium, and triquetral), the heads (distal) and bases (proximal) of the metacarpals (Mc1–Mc5) and phalanges, including all proximal (PP1–PP5) and intermediate phalanges (IP2–IP5), and the distal phalanx (DP1) of the thumb. We exclude the pisiform and non-pollical distal phalanges due to the variable and miniscule trabeculae observed in the μCT scans, which was considered insufficient to allow for a robust calculation of the trabecular parameters (Pahr and Zysset, 2009a; Gross et al., 2012).

Due to shape variation among metacarpals and phalanges, each head/base segment was manually defined prior to analysis. To explore how trabecular structure may reflect differences in joint loading, each metacarpal head/base segment was subdivided into four regions at the radioulnar and dorsopalmar midlines (i.e., dorsoulnar, dorsoradial, palmoulnar, and palmoradial regions) and each phalangeal head/base segment was subdivided into two regions at the radioulnar midline (i.e., radial and ulnar regions). Trabecular parameters for each region were quantified using a Medtool script containing the dimensions of each bone segment.

Statistical analyses

Because of the interdependence of bones and muscles within the hand, we assume that many trabecular measurements may not be independent (e.g., BV/TV in the head of the metacarpal and the base of the articulating proximal phalanx). As such, we statistically tested our hypotheses using linear mixed effect models because they are able to compensate for underlying structures within the data (i.e., varying hierarchies; Lazic, 2010) through the inclusion of random effects within the models (Barr et al., 2013). An example of this would be including the random effect of the ‘individual’ when there is data from bones of the right and left side. Table 2 defines the terms used to describe each model, while Figure 1 illustrates the three levels of comparison (head/base or carpal, metacarpal region, phalangeal region).

To explore variation among the regions of the hand and to help address the problem of non-independence more fully (i.e., reduce type I error), we defined functional groups for certain interrelated bones (e.g., thumb and rays II–V; see SOM S2 for further details). In addition, previous research has shown that there are significant differences between the head/base trabecular architecture of the Mc1, when compared to the Mc2–Mc5 (i.e., greater BV/TV and E with lower DA in the Mc1 head relative to the base while the reverse pattern has been found in the Mc2–Mc5; Lazenby et al., 2011a; Stephens et al., 2015, 2016b). For this reason, we ran models for the thumb bones (trapezium, Mc1, PP1, DP1) separately from the other bones in the hand (carpals, Mc2–Mc5, PP2–PP5, IP2–IP5). Violin plots were generated with the Seaborn v0.8.0 statistical data visualization package to compare distributions between variables (Waskom et al., 2017). All other statistical figures were generated with R v3.3.2 (R Core Team, 2016).

Model implementation

Six separate model setups were used to test for trabecular structure differences across regions of the hand. Each model was fitted using a Gaussian error structure and maximum likelihood (Bolker, 2008) using the lmer function within the lme4 package (Bates et al., 2014) for R. Each of the six model setups contained two models – a ‘hand’ subtype and ‘thumb’ subtype – for each trabecular parameter compared (i.e., the response variables BV/TV, E, and DA).

Models in type 1 were run on data at the level of the bone and bone segment (i.e., metacarpal or phalangeal head and base, or carpal). Models in type 2 were run on data at the level of the metacarpal region (e.g., dorsoradial or palmoulnar regions of the Mc head and base) while models in type 3 used data at the level of the phalangeal region (i.e., radial and ulnar regions of the head and base). Each of these model types were further divided into two subtypes, based on data from the hand (i.e., not including the thumb; subtype a), and data from the thumb only (subtype b). Finally, two models were run for each subtype, one with BV/TV as the response variable and one with E as the response variable. Following Barr et al., (2013), all possible random slopes were included for these models. The specific steps followed for inclusion or rejection of each model are described in SOM S3. In all models, our primary aim was to test specifically for sample differences (post-Neolithic vs. forager) and, where applicable, differences by anatomical region. This included the potential for such differences to vary depending on the combination of sample, segment, and region being considered. In the same models, we also tested for whether there were any patterns across samples and segments or regions that differed based on the functional group being considered, but as these tests did not address our primary aim, the results are presented in SOM S4.

<u>Type 1 model setup segment-level models.</u> The type 1 models included data from bone segments (complete carpals, and metacarpal/phalangeal heads and bases). Subtype 1a included data derived from all bones of the hand, excluding those of the thumb. The two models in subtype 1a, each with a response variable of BV/TV or E, contained the predictors sample (post-

Neolithic vs. forager), segment (head, base, or carpal), side (left or right), and the sample-segment interaction. Additionally, we included random effects of functional group, skeletal element, specimen, hand ID (e.g., Qafzeh9-Left, or Arene Candide2-Right), and specific ID (i.e., identifying the specific bone; Table 2). The two models in subtype 1b included data from the bones of the thumb only, and all test predictors were the same as those in subtype 1a, aside from functional group as a random effect. The test predictors (i.e., the predictors of interest) for all four models in type 1 were sample and the sample-segment interaction. The secondary test predictors (i.e., those involving functional groups) were tested in subtype 1a models only and are described in the SOM S4 for model subtype 1a.

Type 2 model setup metacarpal region-level models. These models included data from the head/base regions of the metacarpals (dorsoulnar, dorsoradial, palmoulnar, palmoradial), with subtype 2a including data from Mc2–Mc5 and subtype 2b including data from Mc1 only. Both models in subtype 2a contained the predictors sample, segment, region (i.e., dorsoradial, dorsoulnar, palmoradial, or palmoulnar), side, and all two- and three-way interactions among sample, segment, and region. The random effects included were functional group, skeletal element, specimen, hand ID, specific ID, and region group (e.g., Qafzeh9-Left-Mc2-Base). The predictors for models in subtype 2b were identical to those in subtype 2a except for the exclusion of functional group and hand ID as random effects. Test predictors were all three- and two-way interactions, sample, and region for all models in type 2. All secondary test predictors from subtype 2a are described in SOM S4.

Type 3 model setup phalangeal region-level models. These included data at the level of the phalangeal head/base regions (ulnar and radial). Subtype 3a incorporated data from PP2–PP5 and IP2–IP5, while subtype 3b incorporated data from PP1 and the base of DP1. Subtype 3a models included as predictors sample, segment, region (i.e., radial or ulnar), side, and all two- and three-way interactions among sample, segment, and region. The random effects were functional group, skeletal element, specimen, hand ID, specific ID, and region group. Subtype 3b models were the same as those in subtype 3a, aside from functional group as a random effect. The test predictors for all type 3 models were identical to those for type 2. The secondary test predictors are described in SOM S4 for model subtype 3a.

Visual analysis

To compare sample differences in the distribution of site-specific BV/TV with morphologies that most closely approximate the actual shape variation between the post-Neolithic and forager bones, we used a custom Python 3.5 (Python Software Foundation) script to chain together slightly modified versions of the methods described in detail previously (Boyer et al., 2015; Gee et al., 2015; Tsegai and Stephens et al., 2017). A detailed illustration of the workflow, along with the specific software packages, is described in SOM S5 and SOM Figure S2**.** In short, we used modules within Medtool to interpolate and map site-specific BV/TV to the nearest elements of the mesh representing the trabecular volume (spacing 0.6 mm). Hereafter, each individual mesh was globally aligned and registered to a representative mesh for each bone (e.g., hamate). The deformation from the registration was then used to generate a statistical shape model (spacing 0.3 mm), which represents the ‘mean-mesh’ (Cootes and Graham, 1995; Joshi et al., 2016). We then registered the mean-mesh to each individual mesh, and the corresponding site-specific BV/TV values at each vertex were then averaged for each sample (e.g., all hamates in the forager sample) and mapped onto the mean-mesh.

Results

SOM Table S2 contains the carpal, metacarpal head/base, and phalangeal head/base mean values and standard deviations for all of the trabecular parameters related to mechanical properties (BV/TV, E, DA) and architecture (Tb.Th, Tb.Sp). The sample means for BV/TV, E, and DA are illustrated by skeletal element in Figure 2, while those of Tb.Th and Tb.Sp are illustrated in Figure 3. A heatmap depicting individual variation for BV/TV, E, and DA by bone and segment is available in SOM Figure S3.

Models with BV/TV and E as the response variable successfully met all the model assumptions, while those for DA were rejected because they did not meet the criteria for normality and homogeneity of residuals (SOM Fig. S4). Therefore, we averaged the right/left DA values for bones belonging to the same individual and performed a Mann-Whitney U pairwise comparison between the post-Neolithic and forager samples for each bone or segment. The significant results for the final models are summarized below, while the results for each of the model comparisons are available in SOM Table S3.

Sample differences in anisotropy

SOM Table S4 contains the results of the Mann-Whitney U comparisons. Significant differences were found for the lunate (post-Neolithic = 0.12, forager = 0.03; $p = 0.043$) and triquetrum (post-Neolithic = 0.10, forager = 0.04; p = 0.028). A trend (i.e. marginal significance) was also identified for the Mc2 base (post-Neolithic = 0.17, forager = 0.12; p = 0.057) and Mc3 base (post-Neolithic = 0.17, forager = 0.10; p = 0.067). In each case this was the result of the post-Neolithic sample being more anisotropic than the foragers, which was the general pattern across the hand in all but the PP1 head, Mc5 head/base, and PP5 head/base. In general, DA was much more variable (i.e., high standard deviations; see SOM Table S2 and SOM Fig. S5) across the hand in both samples, compared with BV/TV and E (see below).

Sample differences in the segments for hand (1a) and thumb (1b) models

Model 1a investigated sample differences in BV/TV and E in bone segments of the hand (scaphoid, lunate, triquetral, hamate, capitate, trapezoid, and Mc2–Mc5, PP2–PP5, and IP2–IP5 head/base segments), while model 1b focused on the bone segments of the thumb (trapezium, Mc1 and IP1 head/base segments, and DP1 base segments). In all four models, we found a significant interaction between sample and segment (hand - BV/TV: p = 0.045; E: p = 0.030; thumb - BV/TV: p = 0.048; E: p = 0.026), indicating that the difference between the two samples varies depending on which segment is being considered (e.g., the difference in the Mc1 is different from that in the trapezium).

The model type 1 results are illustrated in SOM Figure S6. For both BV/TV and E, the forager sample has higher values than the post-Neolithic overall. However, while the differences are similar for the heads and bases, the differences in carpal BV/TV and E are more pronounced (Fig. 2; see also SOM Fig. S3). Figure 2 shows the respective distributions of BV/TV, E, and DA for each carpal in each sample and—while both samples share a pattern of comparatively high BV/TV and E in the lunate, scaphoid, and capitate—the mean values for foragers are greater throughout the carpus. The greatest difference between the mean BV/TV and E for two samples is in the lunate, followed by the triquetral, capitate, and trapezium (see SOM table S2). The violin plots of each carpal illustrate the distributions for BV/TV, E, and DA for each of the two samples (Fig. 4). Given the similarity in mean trabecular spacing between the samples (Fig. 3), the identified interactions for BV/TV and E appear to be driven by generally thicker and more isotropic trabeculae in the carpus of the foragers, which is particularly pronounced in the lunate, capitate, triquetral, and trapezium.

Sample differences in the metacarpal regions for hand (2a) and thumb (2b) models

SOM Table S5 summarizes mean regional values of each sample by respective metacarpal or phalangeal head/base segment. For the models of the hand metacarpal regions (subtype 2a, head/base of Mc2–Mc5: dorsoradial, dorsoulnar, palmoradial, palmoulnar), we found a significant region-sample interaction for both response variables (BV/TV: $p = 0.002$, E: $p = 0.002$) as well as a significant region-segment interaction for BV/TV ($p = 0.013$). In the model of thumb metacarpal regions (subtype 2b, head/base Mc1: dorsoradial, dorsoulnar, palmoradial, palmoulnar), with BV/TV as the response variable we found a significant two-way interaction between sample and region ($p = 0.001$), as well as region and segment ($p < 0.001$), with a trend for the sample-segment interaction ($p = 0.074$). With E as the response variable, there was a trend for the three-way interaction between sample, region, and segment ($p = 0.076$).

Model type 2 results are illustrated in SOM Figures S7 and S8, while the mean BV/TV, E, and DA by head/base region are illustrated in Figure 5. For both samples, the head/base region pattern for BV/TV was very similar across the metacarpals (e.g., greater values in the Mc1 palmoradial region and Mc2–Mc4 palmoulnar region), and there was a tendency for the values in the Mc2 and Mc3 to be comparatively higher. Still, the forager sample showed consistently higher mean values, with the notable exception of the dorsoulnar and dorsoradial regions of the Mc1 base. Between the two samples, the differences were most marked in the palmoradial and palmoulnar regions of both head/base segments of the Mc1–Mc5 when compared to the dorsal regions, and this difference was exaggerated in the Mc2–Mc5 heads (SOM Fig. S7). The pattern for E across regions was, again, fairly similar between the samples for both the metacarpal heads and bases (Fig. 5) with the most striking differences appearing at the palmoulnar and palmoradial regions of the Mc1–Mc5 heads, where the forager sample showed much higher values (see also SOM Fig. S8). Again, there was a notable difference in the Mc1 dorsoulnar region of the base, with the post-Neolithic sample having greater values of E than the foragers.

Most differences between the two samples were related to the disparity between the various metacarpal regions. Architecturally (Fig. 3), there was little difference in mean Tb.Sp between the two samples while mean Tb.Th was notably thicker for the foragers at the base of the Mc3. The most marked differences between the two samples were in the distribution of mean DA among the metacarpal regions, which is relevant because E takes into account the fabric (i.e., the DA) as well as the BV/TV when it is calculated. Interestingly, for both samples the anisotropy pattern between the head/base segments of Mc5 was more similar to that of the Mc1, with the head being more anisotropic than the base. The mean differences in DA by region (Fig. 5) show the foragers being more isotropic in the two palmar regions of the Mc1/Mc5, and two dorsal regions of the Mc3, but all Mc2 regions being anisotropic. At the base of the metacarpals, the forager sample was generally more isotropic in the Mc1–Mc4, but more anisotropic in the two ulnar regions of the Mc5. Taken together, the differences between the two samples were most pronounced in the Mc3 base, the palmar region of the Mc4 head/base, the palmoradial regions of the Mc5 base, and the palmoulnar/dorsoulnar regions of the Mc5 head.

Sample differences in the phalangeal regions for hand (3a) and thumb (3b) models

For hand models in subtype 3a (PP2–PP5 and IP2–IP5 head/base segments), we found that the forager sample had significantly higher BV/TV ($p = 0.018$) and E ($p = 0.016$) in the phalangeal bones of the hand. For thumb models in subtype 3b (PP1 head/base segments, and DP1 base segments), there was a trend for the difference between the samples in BV/TV ($p = 0.059$) and E ($p = 0.059$), with those of foragers being greater for both measures. Further, in thumb model 3b, we found a significant region-segment interaction for BV/TV ($p < 0.001$) and E ($p < 0.001$), where the values in the radial region were found to be higher than those in the ulnar region for both measures, with the variation in head being the most pronounced.

Model type 3 results are illustrated in the SOM Figure S9. Figure 5 shows the regional BV/TV, E, and DA means for each sample by skeletal element and segment, while violin plots comparing the regional differences in BV/TV and E are presented in the SOM Figures S10 and S11. Like the metacarpal regions above, the two samples were similar in that the higher BV/TV and E values, along with lower DA values, were found in the central rays of the hand (rays II–IV). There was also similarity in how BV/TV and E were distributed within the thumb, as suggested by the interaction identified in the pollical phalanges. Here, the values on the radial side were greater than the ulnar side in both samples, which appeared to be driven by the greater E and BV/TV values in the head (SOM Figs. S10 and S11). As in the other bones, the regional means for BV/TV and E were generally greatest in the forager sample, with those in the heads of the various phalanges being the most different between the two samples, while those of the PP1, DP1, and IP5 base were very similar. The greatest disparity between the samples was in rays II, III, and V, particularly the heads of the intermediate phalanges. Architecturally, the two samples share similar Tb.Sp throughout the hand (Fig. 3) and high DA at the base of PP5 and IP2 (Fig. 3). Foragers had greater mean Tb.Th and lower DA in the heads of PP4 and MP4, as well as the PP1 base radial region.

Visualized site-specific BV/TV

Figure 7 presents a palmar and dorsal comparison for each sample of the average surface site-specific BV/TV for each bone analyzed in this study, while an interactive mesh is available in the online version or as a downloadable PLY file (SOM Model S1). There was a general similarity between the two samples, but the forager sample differed in having higher values (darker orange/red), which also tended to encompass a greater surface area than the post-Neolithic sample (the extent of the orange/red borders). Differences between the two samples were particularly marked in the carpals, along ray III, and in the heads of all the phalanges. This is consistent with the statistical analyses reported above, with the forager sample demonstrating significantly greater overall BV/TV and E, with values for DA being significantly different for the lunate and triquetral.

The color map of site-specific BV/TV across the phalanges is consistent with model results 3a and 3b (Fig. 7; also see above and Fig. 6). Both samples showed similarly high BV/TV values and distribution in the pollical phalanges and there was also a similar BV/TV distribution among the non-pollical phalanges, with greater values in the heads relative to the bases. Site-specific BV/TV values were greater in the forager sample overall, with the largest differences between the two samples found at the bases of the phalanges on the dorsal (PP2–PP4 and IP2–IP5) and palmar aspects (PP2–PP4), as well as the heads (PP3 and PP5 head ulnar region).

Figure 8 isolates the articular surfaces of the metacarpal heads and bases, showing patterns of site-specific BV/TV that are generally consistent with the results of metacarpal models 2a and 2b (see above), and the regional averages (Fig. 5). In both samples, the concentrations in the Mc1 were greatest in the radial regions of the head and base, while the heads of the non-pollical metacarpals showed a tendency towards higher values in the palmar-ulnar region. Although BV/TV mean values were, again, generally higher in the foragers, the pattern of BV/TV distribution was similar between the two samples. Compared with the post-Neolithic sample, foragers showed particularly high concentrations of BV/TV at the base of the Mc2 and Mc3, the palmar-radial portion of the Mc1 head, and the palmar-ulnar region of the Mc3 head.

For the hand and thumb models (1a and 1b), the significant differences were the result of variance in the carpals, with the forager sample demonstrating greater overall mean BV/TV and E. This difference was echoed in site-specific BV/TV color maps that highlight the sample variation in the carpals from different anatomical views (Figs. 9 and 10). Along the distal carpal row (trapezoid, capitate, hamate) there were similarities in the distribution of site-specific BV/TV (i.e., ulnar aspect of the trapezoid, capitate head, and the triquetral and capitate facets of the hamate), but the values for the foragers were much higher and more extensive, particularly the radioulnar banding along the capitate head and the trapezoid-capitate articulation (Fig. 10). These high BV/TV patterns correspond with those seen in distal view at the midcarpal joint (Fig. 9), where high values were found in both samples along the dorsal aspect of the lunate and ulnar aspect of the scaphoid articular surfaces, where they cup the capitate head, but the patterns were more pronounced in the forager sample. In proximal view, there were also BV/TV concentrations along the scaphoid and lunate at the radiocarpal joint in both samples (Fig. 9), but with these patterns being much more pronounced in the proximal and palmar surfaces of the lunate, as well as higher BV/TV in the triquetrum, compared with the post-Neolithic sample. The forager sample also had a higher and more extensive BV/TV distribution at the palmoulnar aspect of the trapezium's Mc1 facet, the capitate's Mc3 facet, and the trapezoid's scaphoid facet (Figs. 7 and 9).

Visualized across joint patterns

Figure 11 shows a sagittal cross-sectional image of site-specific BV/TV through the lunate, capitate, and bones of ray III (Mc3, PP3, IP3) for two post-Neolithic males from differing locations but the same time period (19th century). Here the comparison is between individuals with comparatively low (Fig. 11A) and high (Fig. 11B) BV/TV throughout the hand (see SOM Fig. S12 for a comparison of trapezoids from multiple individuals). Along this articular chain there is a good correspondence between the concentrations of relatively high site-specific BV/TV across each joint. Overall the BV/TV distributions between the individuals are similar (e.g., high BV/TV at the palmar metacarpophalangeal joint or dorsal lunate and central capitate head), but the individual with high BV/TV differs in having high concentrations at the palmar capitate-Mc3 joint and in the palmar lunate.

Discussion

We examined the trabecular architecture within 22 of the 27 bones of the human hand from a temporogeographically diverse collection of individuals with the aim of assessing if the structural patterns across the joints were consistent with hand biomechanics. Additionally, we categorized and compared individuals from a post-Neolithic and forager sample to see if the variation between the two samples differed according to presumed differences in manipulative loading. Given the comparable external morphology of recent *H. sapiens* (see Trinkaus, 2016), we predicted that the general trabecular structure and site-specific BV/TV distributions would be consistent with loading during flexion of the interphalangeal joints, flexion with abduction at the metacarpophalangeal joints, and thumb opposition at the metacarpophalangeal and TMC joints. In relation to sample differences, we predicted that the forager sample would have a pattern consistent with higher and more variable manipulatory loading, which would be reflected in higher average BV/TV, E, and lower average DA among the regions of the hand. Furthermore, we predicted that these differences would be reflected in the distribution of site-specific BV/TV, with higher values in the forager hand being consistent with areas of joint contact observed during finger flexion, thumb opposition, and typical wrist movements.

Because previous studies have focused on hand bone trabecular architecture in isolated elements (e.g., the Mc3 head) or limited regions of the hand (e.g., metacarpals; Lazenby et al., 2011a; Zeininger et al., 2011; Schilling et al., 2014; Matarazzo, 2015; Skinner et al., 2015a; Barak et al., 2017; Reina et al., 2017), we first summarize the general trabecular patterns across the hand, and then present results on the non-pollical phalanges, metacarpals II–V, carpals, and thumb. Following this, we discuss the interplay between hand loading, development, demography, and individual variation across our samples.

General pattern

We found support for the predictions of similar hand use and wrist motion in the shared distribution of trabeculae in the carpals, metacarpals, and phalanges of both the post-Neolithic and forager samples. These similarities are suggestive of comparable joint contact and loading as well as overall hand postures during manipulation, which is supported by studies of modern humans showing that a limited number of hand grips are used for most daily tasks (Bullock et al., 2010; Vergara et al., 2014; Liu et al., 2016b). More specifically, both samples demonstrated a general pattern of high BV/TV and E in the heads of the Mc1 and the phalanges, when compared to bases, and in the Mc2–Mc5 bases, when compared to the heads. Both samples also shared a tendency to have relatively high BV/TV and E with lower DA throughout the central portions of the hand (capitate, lunate, scaphoid, Mc2–Mc3, PP2–PP4, IP2–IP4). The site-specific BV/TV for the post-Neolithic and forager samples, as well as the individual meshes (Fig. 11), also showed a good correspondence between concentrations of relatively high BV/TV and areas of expected contact across joints (Figs. 7–11, SOM Fig. S12).

When the forager trabecular structure is compared to that of the post-Neolithic sample, the higher BV/TV, E, Tb.Th, site-specific BV/TV, and lower DA support our prediction that the forager sample would reflect a pattern of higher and more varied loading during hand use. BV/TV and E were significantly higher across the hand, the metacarpal/phalangeal segments, and the metacarpal/phalangeal regions, while DA was significantly lower for the lunate and triquetral (Figs. 2 and 3, SOM Figs. S6–S9). Variation in site-specific BV/TV was consistent with these significant differences, with the forager sample showing higher overall values, with the borders of the high BV/TV extending further across the joint surfaces. These differences were most pronounced in the carpals (scaphoid, lunate, capitate, triquetral, and trapezium), metacarpals (Mc1–Mc5 heads, Mc2–Mc3 bases), and phalanges (heads, and dorsal aspect of bases). These results are generally consistent with previous studies documenting more robust bone structure in upper and lower limb bones in active versus less active human samples (e.g., Stock, 2006; Ryan and Shaw, 2015; Scherf et al., 2016).

Finger phalanges

There is support for our prediction that the phalangeal trabecular structure would reflect flexion at the interphalangeal joints in both samples and that the forager sample would show evidence of greater loading overall. Both samples shared a pattern of relatively high BV/TV and E with low DA in the phalangeal heads when compared to the bases (Figs. 2 and 6, SOM Fig. S5), particularly in the central rays of the hand (II–IV). Higher BV/TV in the palmar regions of the proximal phalanges and dorsal regions of the intermediate phalanges in both samples is consistent with flexion of the interphalangeal joints. In each case, the forager sample had lower DA overall, with significantly higher BV/TV and E throughout the phalanges. Taken together, these results suggest general similarities in finger positioning during loading, but the pattern for the forager sample hints at greater and more varied loading of the fingers, on average. This may be related to variation in finger recruitment strategies, with the higher DA in the post-Neolithic PP4–PP5 and IP2 bases signifying a consistency not present in the forager sample (Fig. 2).

As far as we are aware, no other study has investigated human phalangeal trabecular architecture (for African apes, see Matarazzo, 2015), but in both samples mean BV/TV and E were generally greater in the distal segments of the phalanges (i.e., IP head > PP head; see SOM Fig. S5). Overall this agrees with biomechanical studies measuring higher force and contact pressures in the distal segments of the fingers during manipulation (Williams et al., 2012), power grasping (Kargov et al., 2004; Goislard de Monsabert et al., 2012), and simulated grasping (Chamoret et al., 2016). However, it conflicts with biomechanical modeling and validation studies that report increasingly higher internal joint forces moving distal to proximal along the phalanges (i.e., IP head < PP head < Mc head; Cooney and Chao, 1977; An et al., 1983, 1985). Thus, the head > base distribution of trabecular bone here is seemingly in conflict with the distal < proximal joint force pattern. A partial explanation for this inconsistency may be found in the force attentuation provided by soft tissues and variation in the articular surface areas of the fingers (Rafferty and Ruff, 1994; Ruff, 2002; Diogo et al., 2012; Marzke, 2013; Roberts and Konow, 2013; Hu et al., 2014). Studies quantifying the stiffness and compliance of the fingers have shown how the joint capsules and musculotendon network of the hand act to dissipate mechanical energy during impact to enhance grip stability while preventing injury

(Höppner et al., 2013, 2017; Fujihira et al., 2015; Deshpande et al., 2017). Qiu and Kamper (2014) have also demonstrated that greater joint contact forces occur with more extreme flexion (e.g., 60–90º), and that this force is greater in the distal joints due to the relative reduction in tendon mass towards the fingertips (i.e., the proximal interphalangeal joint > metacarpophalangeal joint). In other words, among the phalanges, manipulative activities that require flexed fingers (i.e., power and precision grips) result in greater force than those with straight fingers. Thus, the inconsistency between higher predicted load but lower trabecular BV/TV and E throughout the phalanges is likely attributable to variation in joint angles during manipulation and, in particular, the relatively large joint surface areas and more massive soft tissue structures towards the proximal portions of the fingers that act to dissipate the higher loads.

Metacarpals II–V

As with the phalanges, we found support for our prediction that both samples would demonstrate similar loading patterns at the metacarpophalangeal and carpometacarpal joints, but with more intense and varied loading in the forager sample. Both post-Neolithic and forager samples generally showed greater mean BV/TV and E in the Mc2–Mc5 bases, when compared to the heads (SOM Fig. S5). They also tended to have greater BV/TV, E, and Tb.Th but lower DA in the central metacarpals (Mc2–Mc3; Figs. 2 and 5). The palmar regions of the Mc1–Mc5 heads and bases had higher BV/TV and E, specifically the palmoulnar regions of Mc2–Mc5, which is consistent with a flexed and adducted joint position of the proximal phalangeal bases as the fingers and thumb rotate towards one another during opposition (Brand and Hollister, 1993). Again, the forager sample showed significantly higher BV/TV and E compared to the post-Neolithic sample, consistent with higher loading. These differences were most pronounced in the palmar regions of the Mc2–Mc4.

Our results are in keeping with previous studies that report an agreement between predicted loading history and metacarpal trabecular structure using VOI (Lazenby et al., 2008b; Chirchir et al., 2017b) and whole bone/epiphyseal methods (Tsegai et al., 2013; Skinner et al., 2015a). Our results contrast with Wong et al. (2017), who found that the dorsal, rather than palmar, region of the Mc2–Mc3 bases had generally higher trabecular bone mass and the Mc4–Mc5 showed a more homogeneous distribution across the base. However, this contradiction likely reflects the differing methodologies; whereas Wong et al. (2017) analyzed single tomographic slices using peripheral quantitative CT, we characterize the entire epiphyses. In the discussion, Wong et al., (2017) suggested that the more homogenous densities were likely related to the force attenuation provided by the tight articulation of the metacarpal bases and supportive ligaments. This interpretation is supported here with our finding of high concentrations of site-specific BV/TV between the Mc2/Mc3 and Mc4/Mc5 (Fig. 8), as well as concentrations along the dorsal surfaces of metacarpal bases that correspond to ligament attachment sites (Fig. 7).

Although the relationship between functional bone adaptation and musculotendon morphology is debatable (Vickerton et al., 2014; Rabey et al., 2015; Wallace et al., 2017a), the high site-specific BV/TV concentrations along the bases of the Mc2, Mc3, and Mc5, and those along the shaft of the Mc1 and Mc5, are consistent with muscle attachment sites related to flexion and opposition (Fig. 7; Brand and Hollister, 1993; Gislason et al., 2009; Diogo and Wood, 2011). For example, those at the palmar base of the Mc3 and along the dorsoradial shaft of the Mc1 and ulnar shaft of the Mc5 correspond to the attachment sites of the oblique head of the adductor pollicis, the opponens pollicis, and opponens digiti minimi respectively, which are thought to increase the mechanical effectiveness of the thumb and fifth finger during flexion (Marzke et al., 1998; Maki and Trinkaus, 2011). Similarly, high site-specific BV/TV along the palmar region of the Mc2 and the dorsal region of the Mc2–Mc3 correspond with the attachment sites of the flexor carpi radialis, extensor carpi radialis longus, and extensor carpi radialis brevis, which are important for controlling wrist flexion-extension and radioulnar deviation (Brand and Hollister, 1993). Considering that trabecular modeling events are found adjacent to the loaded site (Sugiyamat et al., 2010; Schulte et al., 2013; Christen et al., 2014; Cresswell et al., 2016) and that bone resists compressive forces better than tensile forces (Phillips et al., 2015), it may be that these site-specific BV/TV concentrations reflect modeling events initiated by tension transmitted to the bone when the muscles/ligaments work to counterbalance and stabilize the hand during manipulation. This interpretation is in line with other studies that note a relationship between attachment sites and changes in the bone microstructure of the hand (Karakostis and Lorenzo, 2016; Saffar, 2016), as well as Karakostis et al. (2017), who reported a significant relationship between human hand bone enthesis shape and occupations featuring high versus low manual loading.

Although both of our samples showed higher palmoulnar BV/TV, E, and site-specific BV/TV at the Mc2–Mc5 heads, the forager sample showed radial and dorsal expansion of these high values (Figs. 5, 7, and 8). For instance, the Mc5 of the forager sample showed relatively high site-specific BV/TV that extends along the dorsal aspect and ulnar lobe of the head. When paired with the high DA along the dorsal region of the head and palmoulnar region of the base, this suggests a greater consistency in loading while the fifth digit is abducted, which would be consistent with wide grips involving broad/large objects (Goislard de Monsabert et al., 2014). The forager sample also had higher BV/TV, E, and site-specific BV/TV between the Mc2–Mc3 bases and, to a lesser extent, between the Mc4–Mc5 bases (Figs. 5 and 8). Along with the relatively low DA at the base of the Mc2–Mc4 and head of the Mc3, it may be that this pattern represents the distribution of high manipulative loading as the joints stabilize the hand (El-Shennawy et al., 2001; Buffi et al., 2013).

Carpals

For the carpals, both samples tended to have high values of BV/TV, E, and lower DA in the central elements (i.e., capitate, lunate, scaphoid; Fig.2) and similar distributions of site-specific BV/TV among the radiocarpal and midcarpal joints (Figs. 9 and 10), supporting our prediction of comparable patterns of joint contact. Our prediction regarding higher and more variable manual loading for the forager sample was supported by the significantly higher BV/TV, E, and lower DA in the carpals, as well as the visibly higher site-specific BV/TV concentrations observed along the scaphoid, lunate, capitate, and triquetral (Figs. 2, 9 and 10).

In relation to the predictions of wrist movement, the concentrations of site-specific BV/TV at the radiocarpal (proximal lunate and scaphoid) and midcarpal joints (distal lunate, distal scaphoid, and capitate head) are consistent with the load transfer and kinematics observations of carpals in motion (e.g., Crisco et al., 2005; Majima et al., 2008; Gislason et al., 2009, 2010; Rainbow et al., 2013; Márquez-Florez et al., 2015). More specifically, this pattern is consistent with the kinematics of the carpals when moving between radial-extension and ulnar-flexion as the wrist moves through the ‘dart-thrower’s’ motion, which balances the tension between the carpals in a manner that emphasizes motion at the midcarpal joint while minimizing motion at the radiocarpal joint (Moojen et al., 2002a; Edirisinghe et al., 2014; Rainbow et al., 2015). This movement characterizes the path that the wrist travels during many high load tasks, such as short swing hammering, clubbing, and hard hammer knapping (Leventhal et al., 2010; Garg et al., 2014; Williams et al., 2014), and is consistent with the pattern of extremely low DA, high BV/TV, E, and Tb.Th in the forager capitate, lunate, and scaphoid.

Following from this, the extremely low DA and high site-specific BV/TV in the forager triquetral compared with the post-Neolithic sample may stem from loads incurred while stabilizing the wrist during forceful manipulative activities. The high BV/TV on the palmoulnar aspect of the triquetrum (Figs. 7 and 9) is consistent with attachment sites of the ligaments that help to stabilize the ulnar wrist (Saffar, 2016). Similarly, the high BV/TV, E, and extremely low DA for the trapezoid, capitate, and Mc2–Mc3 bases are consistent with derived articular configuration of the *Homo* radial carpometacarpal complex, which helps distribute the high joint reaction forces from the thumb (i.e., Mc3 styloid, and reoriented Mc2/trapezoid/trapezium angles; Marzke, 1983, 1997; Tocheri et al., 2003, 2005, 2008; Ward et al., 2014). More specifically, the presence of higher site-specific BV/TV values in the forager trazpezoid-capitate articulation and those through the palmar aspect of the trapezoid (Fig. 10 and SOM Fig. S12) agree with the manner in which load is suggested to pass transerversly through the expanded palmar aspect of the trapezoid during strong pinch/power grip (Tocheri et al., 2005; Marzke et al., 2010).

Thumb

Both post-Neolithic and forager samples showed higher relative BV/TV and E in the palmar and palmoradial regions of the Mc1, the radial regions of the pollical phalanges, and high site-specific BV/TV at the trapeziometacarpal joint (Figs. 2, 6, and 9), which together are consistent with the motion of the thumb during opposition to the other fingers (Nufer et al., 2008; Lee et al., 2013; Ladd et al., 2014; D'Agostino et al., 2017). High site-specific BV/TV in the palmar regions of the Mc1 is consistent with the area of joint contact at the TMC when the thumb is opposed (Schneider et al., 2017), as well as the results of previous studies (Skinner et al., 2015a; Stephens et al., 2016a; Wong et al., 2017). In contrast to other anatomical regions of the hand, we did not find significant differences between the samples in levels of BV/TV and E for the Mc1 or phalanges. While this suggests that thumb use was more similar for the two samples than originally anticipated, the forager sample did show significantly higher BV/TV and E in the trapezium (SOM Fig. S6). Furthermore, the high site-specific BV/TV expands further across the trapezium's Mc1 articular surface and palmodorsally along the scaphoid articular surface (Figs. 9 and 10). This pattern is consistent with the motion described by D'Agostino et al., (2017), where the Mc1 base rotates during opposition of the thumb while the dorsoradial ligament tightens in such a way that the palmar beak of the Mc1 base locks against the palmoulnar region of the trapezium to stabilize the joint. When the higher regional BV/TV and E in the palmar regions of the Mc1 base and the greater site-specific BV/TV on the palmoradial aspect of the Mc1 base and head (Figs. 5, 7-9) are considered together, it may reflect loading involving a widely abducted thumb (e.g., grasping a baseball as opposed to a pinch grip; Halilaj et al., 2013, 2014). Given the specialized thenar musculature of the human thumb compared with other primates (Diogo et al., 2012) —and the force-attenuating properties of soft tissue discussed above—the higher E and BV/TV in the trapezium of the forager sample may reflect higher loading of the thumb overall, with the joint contact forces ultimately being transferred into the broad trapezial Mc1 facet, through to the scaphoid, and into the radius (Marzke et al., 2010). This interpretation would be consistent with a similar transfer of kinetic energy during power grips or strong pinch grips (Tocheri et al., 2003, 2005), as well the results discussed for the remaining carpals above (e.g., the capitate-scaphoid border of the trapezoid).

Developmental patterns

Although our results are generally consistent with our predictions based on hand kinematics, there are additional factors, such as ontogeny, that can influence trabecular structure (Ryan et al., 2017). For instance, we found the metacarpal/phalangeal head and base differences for BV/TV and E to be fairly uniform across individuals (see SOM Figs. S3 and S5), which could be explained, at least in part, by development. Here the head/base distribution mirrors the position of growth plates, which are located at the base of Mc1 and phalanges and Mc2–Mc5 heads (Rolian, 2016; Perchalski et. al., 2017). Because new trabeculae are formed only within the growth plate (Schulte et al., 2011), it seems somewhat contradictory that the segments opposite the respective plates have the higher relative BV/TV, E, and Tb.Th (i.e., Mc1/phalangeal heads and Mc2–Mc5 bases; Figs. 2 and 3). For the phalanges this could represent a biomechanical trade-off between epiphyseal cortical and trabecular bone (e.g., thicker PP1 base cortical bone allowing for lower BV/TV and E relative to the head). However, Stephens et al. (2016b) found that these trabecular parameters covaried in human metacarpals, such that higher BV/TV and E was paired with a thicker cortex in the Mc1 base and Mc2–Mc5 heads relative to their opposing segments.

In comparison to other primates, Matarazzo (2015) found that the trabecular structure of the extant ape and macaque ray III (Mc3, PP3, and IP3) had a similar tendency for higher BV/TV in the metacarpal/phalangeal heads when compared to the bases. However, there was also substantial overlap in BV/TV values, with some individuals having higher BV/TV in the bases, rather than the heads. While this difference may reflect systemic differences in trabecular structure between humans and non-human primates (Tsegai et al., 2018) or methodology (i.e., whole-bone/epiphysis approach vs. VOI), it may also reflect the high locomotor loading of non-human primate hands compared with that of humans (Marchi, 2005; Marzke et al., 2015). Since non-human primates have the same growth plate locations as humans, this would suggest that loading can supersede a developmental predisposition. For the human metacarpal/phalanges here, there are some BV/TV and E values that are nearly equal between the head/base segments, with three phalanges where the base values are greater than those of the head (SOM Fig. S5). This may mean that loads incurred during manipulation are not high enough to cause frequent head/base variation, or that modeling is superimposed onto the developmental architecture because typical loading of the hand follows this particular pattern (e.g., higher joint force at the distal phalanges; Perchalski et al., 2017; Reina, 2007). In either case, because modeling is limited to modulating trabecular thickness, spacing, and orientation following epiphyseal fusion (Schulte et al., 2011; Barak et al., 2017), there is, at the very least, support for localized modeling among the differing Tb.Th, BV/TV, E, and site-specific BV/TV values (e.g., capitate, lunate, phalangeal heads, Mc3 base; Figs. 2 and 3). Still, these claims would be better substantiated if compared to a similar study involving an ontogenetic sample of human and non-human primates. Comparisons with foot bone trabecular structure, which have identical growth plate positions, could further test the influence of bone development on adult trabecular structure.

Demography and degree of anisotropy

Regarding comparisons of trabecular structure between the two samples, the results for DA are the most difficult to interpret because DA varies considerably compared to all other trabecular parameters (Tables 3 and 5, SOM Fig. S3). In other studies of human trabecular structure, the standard deviations of DA are generally low and comparable to those of BV/TV or Tb.Th, especially in the hands (e.g., Lazenby et al., 2008a, b, 2011a; Barak et al., 2017). Because DA characterizes the relative organization of trabeculae in 3D space—which will differ according to the anatomical region being analyzed—the high variability of DA we report likely relates to the methodological approach (Kivell et al., 2011b; Lazenby et al., 2011b). Namely, those that use single VOIs (Lazenby et al., 2008a, b, 2011a; Barak et al., 2017) versus other studies quantifying DA within the entire bone or epiphysis (Tsegai et al., 2013; Skinner et al., 2015a; Stephens et al., 2016), where the DA variation is similarly high. Considering the DA in the metacarpals here, where the larger bases vary more than the smaller heads (e.g., Mc2–Mc3), it may even be that larger volumes overgeneralize the measure. Being that controlled animal studies demonstrate how struts align with loading axes (Pontzer et al., 2006; Barak et al., 2011), it may be more informative to visualize local differences in DA along with direction of alignment, which should reflect the primary direction of loading between joints (e.g., Tsegai et al., 2013; Barak et al., 2017).

That said, the bimodal distribution in the post-Neolithic carpals suggests a tendency towards either high or low DA (Fig. 4) that requires further investigation, ideally on osteological samples with known biological and occupational information. While we excluded all pathological bones and did not knowingly include individuals of advanced age, it may be that the high DA found in some individuals reflects age or physiological stress-related bias, which is characterized by low BV/TV and high DA (Agarwal, 2004, 2016; Beauchesne, 2017). When considering the large temporal differences between individuals in both samples, and the prevalence of nutritional stress/pathology regardless of subsistence strategy (e.g., Trinkaus et al., 2001; Macintosh et al., 2016), this is likely to have influenced the trabecular structure for some of the individuals in our sample. The inability of this analysis to both control for potentially confounding effects due to a lack of specific life history data (e.g., exact age, sex, occupation), as well as run linear mixed effect models on DA further complicates parsing out these fine-grained differences.

Further limitations

Although the aim of this study was to investigate for the first time the general patterns of trabecular structure across the human hand, there are several limitations to this study, in addition to ones discussed above, that should be underscored when considering the interpretations above. Foremost are the limitations with our sample. As discussed above, we divided up our sample into two broadly-defined groups that are temporogeographically diverse and are not associated with direct life history information. Future analyses on a contemporary sample or well-documented and temporally constrained archaeological sample would be useful to see if the general patterns found here still hold (Karakostis et al., 2017; Reina et al., 2017; Wong et al., 2017). Furthermore, one must consider bias stemming from preservation, such that there are fewer individuals to be sampled in earlier time periods. This dearth of samples complicates the number of reasonable divisions available during analysis, and we must keep in mind that the earlier individuals may not truly be 'representative' of a particular population or time period. For example, the forager individuals that overlap geographically, but not necessarily temporally, show similar values, with Qafzeh 8 and 9 (130–80 ka) having comparable values to the post-Neolithic means, while Arene Candide 2 (11–9 ka) and Barma Grande 2 (24 ka) do not (SOM Fig. S3). While this is interesting and may be related to similarities in terrain, culture, and/or genetic background, it is not a question that can be adequately explored with the limited amount of Pleistocene remains available.

In relation to broader comparisons, we did not explore potential sex-related differences in hand use. Bimanual humeral loading appears to have dramatically increased for females compared to males following the adoption of agriculture (Macintosh et al., 2014, 2017; Sládek et al., 2016), and it may be possible to assess if the right and left hands of females and males from this period differed in consistent ways. Similarly, the functional interpretations here would be better informed if accompanied by comparable data on non-human primate trabecular bone. Although previous studies of isolated hand elements in non-human primates (e.g., Lazenby et al., 2011a; Schilling et al., 2013; Matazarro et al., 2015; Stephens et al., 2016a) generally support the distinctive patterns of trabecular structure reported here for human hands, such a comparison would allow for a more direct assessment of which aspects relate to function and which relate to developmental, genetic, and/or age-related factors (e.g., Barak et al., 2013; Ryan and Shaw, 2015; Agarwal, 2016).

Methodologically, it should be noted that calculation of E in this study is based on computational simulations approximating μFE models experimentally validated using bones other than those of the hand (e.g., femurs/vertebrae; Pahr and Zysset, 2009a,b; Schwiedrzik et al., 2016). Further, while many of the trabecular patterns we found are consistent with what is known about the biomechanics of the human hand, some functional interpretations are based on simplified kinematic models due to the complexity of, for example, carpal movement (Crisco et al., 2005; Gislason et al., 2009), and many of the complex interrelationships between hard and soft tissues of the hand remain poorly understood (e.g., Landsmeer, 1955; Napier, 1960; Crisco et al., 2005; Orr et al., 2010; Kivell et al., 2013; Saffar, 2016; Orr, 2017). Additionally, we did not analyze variation in cortical bone, which has been shown to covary with trabecular variables and is critical to how load is dissipated during manipulation (Tommasini et al., 2009; Stephens et al., 2016b). While beyond the scope of this study, it would be fruitful to compare individual site-specific BV/TV distributions to overlapping maps of DA, local orientation, Tb.Sp., Tb.Th., and cortical bone thickness (e.g., Tsegai et al., 2013; Barak et al., 2017; Tsegai and Stephens et al., 2017), to gain a more holistic functional understanding of variation in bone form.

Conclusions

This study aimed to describe for the first time the general patterns of trabecular structure across the human hand skeleton. The quantitative results and trabecular patterning described here were in line with our predictions of similar hand function between the post-Neolithic and forager samples. Higher BV/TV and E but generally lower DA in the forager sample suggests more intense and varied loading of the hands, on average. Using the site-specific BV/TV maps, we found good correspondence between the articulated elements of the hand, which helped to provide more in-depth interpretations of the quantitative data. Furthermore, the high site-specific BV/TV values were also consistent with the loading expected from in vivo observations of hand use. As such, analysis of trabecular structure and visualization of site-specific BV/TV across the human hand is both useful and relevant to debates about the reconstruction of manipulative behaviors in past samples and may be useful for interpreting fossil hominin remains. However, the functional interpretations made here should be tested on contemporary or archaeological samples of known behavior, and preferably within a broader comparative context of non-human primates.

Acknowledgements

This work was supported by the Max Planck Society (N.B.S., M.M.S., T.L.K., J.J.H.) and the European Research Council Starting Grant (grant number 336301; T.L.K. and M.M.S.). We are grateful for the samples provided by the Research Centre for Palaeolithics and Palaeoethnology, Věstonice (Jiří Svoboda), Museo Nazionale Preistorico dei Balzi Rossi (Elisabetta Starnini), the Museo Archeologico del Finale (Andrea De Pascale), the Sackler School of Medicine at Tel Aviv University (Israel Herskovitz, Alon Barash, and Yoel Rak), Naturhistorisches Museum Wien (Maria Teschler-Nicola and Ronald Muehl), the University of Florence (Jacopo Moggi-Cecchi and Silvia Bortoluzzi), University of Kent (Chris Deter and Patrick Mahoney), and the Johann-Friedrich-Blumenbach-Institut für Zoologie und Anthropologie der Georg-August-Universität Göttingen (Birgit Großkopf). For scanning assistance, we thank David Plotzki and Heiko Temming. For insightful discussions, we thank Colleen Stephens, Adam van Casteren, and Zewdi Tsegai. We thank three anonymous reviewers and the editors of JHE for comments that allowed for a much more nuanced interpretation of the results.

References

Agarwal, S.C., 2016. Bone morphologies and histories: Life course approaches in bioarchaeology. American Journal of Physical Anthropology 159 S61, 130–149.

Agarwal, S.C., Dumitriu, M., Tomlinson, G.A., Grynpas, M.D., 2004. Medieval trabecular bone architecture: the influence of age, sex, and lifestyle. American Journal of Physical Anthropology 124, 33–44.

Alba, D.M., Moyà-Solà, S., Kohler, M., 2003. Morphological affinities of the *Australopithecus afarensis* hand on the basis of manual proportions and relative thumb length. Journal of Human Evolution 44, 225–254.

Almécija, S., Alba, D.M., 2014. On manual proportions and pad-to-pad precision grasping in Australopithecus afarensis. Journal of Human Evolution 73, 88–92.

Almécija, S., Moyà-Solà, S., Alba, D.M., 2010. Early origin for human-like precision grasping: a comparative study of pollical distal phalanges in fossil hominins. PLoS One 5, e11727.

Almécija, S., Alba, D.M., Moyà-Solà, S., 2012. The thumb of Miocene apes: new insights from Castell de Barbera (Catalonia, Spain). American Journal of Physical Anthropology 148, 436–450.

Almécija, S., Orr, C.M., Tocheri, M.W., Patel, B.A., Jungers, W.L., 2015a. Exploring phylogenetic and functional signals in complex morphologies: the hamate of extant anthropoids as a test-case study. The Anatomical Record 298, 212–229.

Almécija, S., Wallace, I.J., Judex, S., Alba, D.M., Moyà-Solà, S., 2015b. Comment on "Human-like hand use in *Australopithecus africanus*". Science 348, 1101.

An, K.N., Ueba, Y., Chao, E.Y., Cooney, W.P., Linscheid, R.L., 1983. Tendon excursion and moment arm of index finger muscles. Journal of Biomechanics 16, 419–425.

An, K.N., Chao, E.Y., Cooney, W.P., Linscheid, R.L., 1985. Forces in the normal and abnormal hand. Journal of Orthopaedic Research 3, 202–211.

Ashley-Montagu, F.M., 1931. On the primate thumb. American Journal of Physical Anthropology 15, 291–314.

Bain, G.I., Clitherow, H.D., Millar, S., Fraysse, F., Costi, J.J., Eng, K., McGuire, D.T., Thewlis, D., 2015. The effect of lunate morphology on the 3-dimensional kinematics of the carpus. Journal of Hand Surgery 40, 81–89.e1.

Barak, M.M., Lieberman, D.E., Hublin, J.J., 2011. A Wolff in sheep's clothing: trabecular bone adaptation in response to changes in joint loading orientation. Bone 49, 1141–1151.

Barak, M.M., Lieberman, D.E., Hublin, J.J., 2013. Of mice, rats and men: trabecular bone architecture in mammals scales to body mass with negative allometry. Journal of Structural Biology 183, 123–131.

Barak, M.M., Sherratt, E., Lieberman, D.E., 2017. Using principal trabecular orientation to differentiate joint loading orientation in the 3rd metacarpal heads of humans and chimpanzees. Journal of Human Evolution 113, 173–182.

Bardo, A., Borel, A., Meunier, H., Guery, J.P., Pouydebat, E., 2016. Behavioral and functional strategies during tool use tasks in bonobos. American Journal of Physical Anthropology 161, 125–140.

Bardo, A., Pouydebat, E., Meunier, H., 2015. Do bimanual coordination, tool use, and body posture contribute equally to hand preferences in bonobos? Journal of Human Evolution 82, 159–169.

Barr, D.J., Levy, R., Scheepers, C., Tily, H.J., 2013. Random effects structure for confirmatory hypothesis testing: Keep it maximal. Journal of Memory and Language 68, 255–278.

Bates, D., Mächler, M., Bolker, B., Walker, S., 2015. Fitting linear mixed-effects models using lme4. Journal of Statistical Software 67, 1—48.

Beauchesne, P., Agarwal, S.C., 2017. A multi-method assessment of bone maintenance and loss in an Imperial Roman population: Implications for future studies of age-related bone loss in the past. American Journal of Physical Anthropology 164, 41–61.

Boesch, C., Boesch, H., 1993. Different hand postures for pounding nuts with natural hammers by wild chimpanzees. In: Preuschoft, H., Chivers, D.J. (Eds.), Hands of Primates. Springer Vienna, Vienna, pp. 31–43.

Bolker, B.M., 2008. Ecological Models and Data in R. Princeton University Press, Princeton.

Borel, A., Chèze, L., Pouydebat, E., 2016. Sequence analysis of grip and manipulation during tool using tasks: a new method to analyze hand use strategies and examine human specificities. Journal of Archaeological Method and Theory 24, 751–775.

Boyer, D.M., Puente, J., Gladman, J.T., Glynn, C., Mukherjee, S., Yapuncich, G.S., Daubechies, I., 2015. A new fully automated approach for aligning and comparing shapes. The Anatomical Record 298, 249–276.

Boyer, D.M., Yapuncich, G.S., Chester, S.G., Bloch, J.I., Godinot, M., 2013. Hands of early primates. American Journal of Physical Anthropology 152 S57, 33–78.

Brand, C.M., Marchant, L.F., Boose, K.J., White, F.J., Rood, T.M., Meinelt, A., 2017. Laterality of grooming and tool use in a group of captive bonobos (*Pan paniscus*). Folia Primatologica 88, 210–222.

Brand, P.W., Hollister, A., 1993. Clinical Mechanics of the Hand. Mosby Year Book, St. Louis.

Buffi, J.H., Crisco, J.J., Murray, W.M., 2013. A method for defining carpometacarpal joint kinematics from three-dimensional rotations of the metacarpal bones captured in vivo using computed tomography. Journal of Biomechanics 46, 2104–2108.

Bullock, I.M., Zheng, J.Z., De La Rosa, S., Guertler, C., Dollar, A.M., 2013. Grasp frequency and usage in daily household and machine shop tasks. IEEE Transaction on Haptics 6, 296-308.

Bush, M.E., Lovejoy, C.O., Johanson, D.C., Coppens, Y., 1982. Hominid carpal, metacarpal, and phalangeal bones recovered from the Hadar formation: 1974-1977 collections. American Journal of Physical Anthropology 57, 651–677.

Cardozo, D.F., Plata, G.V., Casas, J.A., Rodriguez, N.S., 2016. Acute dislocation of the metacarpal-trapezoid joint. Clinics in Orthopedic Surgery 8, 223–227.

Chamoret, D., Bodo, M., Roth, S., 2016. A first step in finite-element simulation of a grasping task. Computer Assisted Surgery 21, 22–29.

Chen, Y.R., Wu, Y.F., Tang, J.B., Giddins, G., 2014. Contact areas of the scaphoid and lunate with the distal radius in neutral and extension: correlation of falling strategies and distal radial anatomy. Journal of Hand Surgery Europe 39, 379–383.

Chirchir, H., 2015. A comparative study of trabecular bone mass distribution in cursorial and non-cursorial limb joints. The Anatomical Record 298, 797–809.

Chirchir, H., Ruff, C.B., Junno, J.A., Potts, R., 2017a. Low trabecular bone density in recent sedentary modern humans. American Journal of Physical Anthropology 162, 550–560.

Chirchir, H., Zeininger, A., Nakatsukasa, M., Ketcham, R.A., Richmond, B.G., 2017b. Does trabecular bone structure within the metacarpal heads of primates vary with hand posture? Comptes Rendus Palevol 16, 533–544.

Christen, P., Ito, K., Ellouz, R., Boutroy, S., Sornay-Rendu, E., Chapurlat, R.D., van Rietbergen, B., 2014. Bone remodelling in humans is load-driven but not lazy. Nature Communications 5, 4855.

Christen, P., Muller, R., 2017. In vivo visualisation and quantification of bone resorption and bone formation from time-lapse imaging. Current Osteoporosis Reports 15, 311–317.

Churchill, S.E., Formicola, V., 1997. A case of marked bilateral asymmetry in the upper limbs of an upper palaeolithic male from Barma Grande (Liguria), Italy. International Journal of Osteoarchaeology 7, 18–38.

Coleman, C., 2003. “Digital inking”: how to make perfect line drawings on computers. Organisms Diversity and Evolution 3, 303–304.

Congdon, K.A., Ravosa, M.J., 2016. Get a grip: substrate orientation and digital grasping pressures in strepsirrhines. Folia Primatologica 87, 224–243.

Cooney, W.P., 3rd, Chao, E.Y., 1977. Biomechanical analysis of static forces in the thumb during hand function. Journal of Bone and Joint Surgery 59, 27–36.

Cootes, T.F., Taylor, C.J., Cooper, D.H., Graham, J., 1995. Active Shape Models-Their Training and Application. Computer Vision Image and Understanding 61, 38-59.

Cowin, S.C., 1985. The relationship between the elasticity tensor and the fabric tensor. Mechanics of Materials 4, 137–147.

Cowin, S.C., Hart, R.T., Balser, J.R., Kohn, D.H., 1985. Functional adaptation in long bones: establishing in vivo values for surface modeling rate coefficients. Journal of Biomechanics 18, 665–684.

Cresswell, E.N., Goff, M.G., Nguyen, T.M., Lee, W.X., Hernandez, C.J., 2016. Spatial relationships between bone formation and mechanical stress within cancellous bone. Journal of Biomechanics 49, 222–228.

Crisco, J.J., Coburn, J.C., Moore, D.C., Akelman, E., Weiss, A.P., Wolfe, S.W., 2005. In vivo radiocarpal kinematics and the dart thrower's motion. Journal of Bone and Joint Surgery 87, 2729–2740.

Currey, J.D., 2011. The structure and mechanics of bone. Journal of Materials Science 47, 41–54.

Cutkosky, M.R., Howe, R.D., 1990. Human grasp choice and robotic grasp analysis. In: Venkataraman, S.T., Iberall, T. (Eds.), Dextrous Robot Hands. Springer-Verlag, New York, pp. 5–31.

D'Agostino, P., Dourthe, B., Kerkhof, F., Stockmans, F., Vereecke, E.E., 2017. In vivo kinematics of the thumb during flexion and adduction motion: Evidence for a screw-home mechanism. Journal of Orthopaedic Research 35, 1556–1564.

Daver, G., Berillon, G., Grimaud-Herve, D., 2012. Carpal kinematics in quadrupedal monkeys: towards a better understanding of wrist morphology and function. Journal of Anatomy 220, 42–56.

Daver, G., Berillon, G., Jacquier, C., Ardagna, Y., Yadeta, M., Maurin, T., Souron, A., Blondel, C., Coppens, Y., Boisserie, J. R., in press. New hominin postcranial remains from locality OMO 323, Shungura Formation, Lower Omo Valley, southwestern Ethiopia. Journal of Human Evolution. https://doi.org/10.1016/j.jhevol.2018.03.011.

Demes, B., Stern, J.T., Jr., Hausman, M.R., Larson, S.G., McLeod, K.J., Rubin, C.T., 1998. Patterns of strain in the macaque ulna during functional activity. American Journal of Physical Anthropology 106, 87–100.

Deshpande, A., Niehues, T., Rao, P., 2017. Implementation of human-like joint stiffness in robotics hands for improved manipulation. In: Ueda, J., Kurita, Y. (Eds.), Human Modelling for Bio-Inspired Robotics. Academic Press, London, pp. 3–35.

Diogo, R., Richmond, B.G., Wood, B., 2012. Evolution and homologies of primate and modern human hand and forearm muscles, with notes on thumb movements and tool use. Journal of Human Evolution 63, 64–78.

Diogo, R., Wood, B., 2011. Soft-tissue anatomy of the primates: phylogenetic analyses based on the muscles of the head, neck, pectoral region and upper limb, with notes on the evolution of these muscles. Journal of Anatomy 219, 273–359.

Domínguez-Rodrigo, M., Pickering, T.R., Almécija, S., Heaton, J.L., Baquedano, E., Mabulla, A., Uribelarrea, D., 2015. Earliest modern human-like hand bone from a new >1.84-million-year-old site at Olduvai in Tanzania. Nature Communications 6, 7987.

Doran, D.M., 1993. Comparative locomotor behavior of chimpanzees and bonobos: the influence of morphology on locomotion. American Journal of Physical Anthropology 91, 83–98.

Doube, M., Klosowski, M.M., Wiktorowicz-Conroy, A.M., Hutchinson, J.R., Shefelbine, S.J., 2011. Trabecular bone scales allometrically in mammals and birds. Proceedings of the Royal Society B 278, 3067–3073.

Dr. Pahr Ingenieurs e.U., 2017. Medtool v4.0. Dr. Pahr Ingenieurs e.U., Pfaffstätten. http://www.dr-pahr.at.

Drapeau, M.S., 2015. Metacarpal torsion in apes, humans, and early *Australopithecus*: implications for manipulatory abilities. PeerJ. 3, e1311.

Edirisinghe, Y., Troupis, J.M., Patel, M., Smith, J., Crossett, M., 2014. Dynamic motion analysis of dart throwers motion visualized through computerized tomography and calculation of the axis of rotation. Journal of Hand Surgery Europe 39, 364–372.

El-Shennawy, M., Nakamura, K., Patterson, R.M., Viegas, S.F., 2001. Three-dimensional kinematic analysis of the second through fifth carpometacarpal joints. Journal of Hand Surgery 26, 1030–1035.

Eren, M.I., Lycett, S.J., 2012. Why Levallois? A morphometric comparison of experimental "preferential" Levallois flakes versus debitage flakes. PLoS One 7, e29273.

Fabre, A.C., Marigó, J., Granatosky, M.C., Schmitt, D., 2017. Functional associations between support use and forelimb shape in strepsirrhines and their relevance to inferring locomotor behavior in early primates. Journal of Human Evolution 108, 11–30.

Fairfield, H., Rosen, C.J., Reagan, M.R., 2017. Connecting bone and fat: the potential role for sclerostin. Current Molecular Biology Reports 3, 114–121.

Falk, D., 1980. Language, handedness, and primate brains: did the australopithecines sign? American Anthropologist 82, 72–78.

FEI Science Visualization Group, 2017. Avizo 9.0. FEI Science Visualization Group, Hillsboro. http://www.fei.com.

Formicola, V., Frayer, D.W., Heller, J.A., 1990. Bilateral absence of the lesser trochanter in a late Epigravettian skeleton from Arene Candide (Italy). American Journal of Physical Anthropology 83, 425–437.

Freivalds, A., 2011. Biomechanics of the Upper Limbs: Mechanics, Modeling and Musculoskeletal Injuries, 2nd ed. CRC press, New York.

Friedl, L., Eisova, S., Holliday, T.W., 2016. Re-evaluation of Pleistocene and Holocene long bone robusticity trends with regards to age-at-death estimates and size standardization procedures. Journal of Human Evolution 97, 109–122.

Frost, H.M., 1987. Bone “mass” and the “mechanostat”: a proposal. The Anatomical Record 219, 1–9.

Fujihira, Y., Harada, K., Tsuji, T., Watanabe, T., 2015. Experimental investigation of effect of fingertip stiffness on resistible force in grasping. In: 2015 IEEE International Conference on Robotics and Automation (ICRA). IEEE, Seattle, pp. 4334–4340.

Gabra, J.N., Li, Z.M., 2016. Three-dimensional stiffness of the carpal arch. Journal of Biomechanics 49, 53–59.

Garg, R., Kraszewski, A.P., Stoecklein, H.H., Syrkin, G., Hillstrom, H.J., Backus, S., Lenhoff, M.L., Wolff, A.L., Crisco, J.J., Wolfe, S.W., 2014. Wrist kinematic coupling and performance during functional tasks: effects of constrained motion. Journal of Hand Surgery 39, 634–642.e1.

Gee, A.H., Treece, G.M., 2014. Systematic misregistration and the statistical analysis of surface data. Medical Image Analysis 18, 385–393.

Gee, A.H., Treece, G.M., Tonkin, C.J., Black, D.M., Poole, K.E., 2015. Association between femur size and a focal defect of the superior femoral neck. Bone 81, 60–66.

Gislason, M.K., Nash, D.H., Nicol, A., Kanellopoulos, A., Bransby-Zachary, M., Hems, T., Condon, B., Stansfield, B., 2009. A three-dimensional finite element model of maximal grip loading in the human wrist. In: Proceedings of the Institution of Mechanical Engineers. Part H. Journal of Engineering in Medicine 223, 849–861.

Gislason, M.K., Stansfield, B., Nash, D.H., 2010. Finite element model creation and stability considerations of complex biological articulation: The human wrist joint. Medical Engineering and Physics 32, 523–531.

Godinot, M., Beard, K.C., 1991. Fossil primate hands: A review and an evolutionary inquiry emphasizing early forms. Human Evolution 6, 307–354.

Goislard de Monsabert, B., Rossi, J., Berton, E., Vigouroux, L., 2012. Quantification of hand and forearm muscle forces during a maximal power grip task. Medicine and Science in Sports and Exercise 44, 1906–1916.

Goislard de Monsabert, B., Vigouroux, L., Bendahan, D., Berton, E., 2014. Quantification of finger joint loadings using musculoskeletal modelling clarifies mechanical risk factors of hand osteoarthritis. Medical Engineering and Physics 36, 177–184.

Green, D.J., Gordon, A.D., 2008. Metacarpal proportions in *Australopithecus africanus*. Journal of Human Evolution 54, 705–719.

Gross, T., Kivell, T.L., Skinner, M.M., Nguyen, N.H., Pahr, D.H., 2014. A CT-image-based framework for the holistic analysis of cortical and trabecular bone morphology. Palaeontologia Electronica 17, 33A.

Gross, T., Pahr, D.H., Peyrin, F., Zysset, P.K., 2012. Mineral heterogeneity has a minor influence on the apparent elastic properties of human cancellous bone: a SRmuCT-based finite element study. Computer Methods in Biomechanics and Biomedical Engineering 15, 1137–1144.

Haïat, G., Padilla, F., Svrcekova, M., Chevalier, Y., Pahr, D., Peyrin, F., Laugier, P., Zysset, P., 2009. Relationship between ultrasonic parameters and apparent trabecular bone elastic modulus: a numerical approach. Journal of Biomechanics 42, 2033–2039.

Halilaj, E., Moore, D.C., Patel, T.K., Ladd, A.L., Weiss, A.P., Crisco, J.J., 2015. Early osteoarthritis of the trapeziometacarpal joint is not associated with joint instability during typical isometric loading. Journal of Orthopaedic Research 33, 1639–1645.

Halilaj, E., Rainbow, M.J., Got, C., Schwartz, J.B., Moore, D.C., Weiss, A.P., Ladd, A.L., Crisco, J.J., 2014. In vivo kinematics of the thumb carpometacarpal joint during three isometric functional tasks. Clinical Orthopaedics and Relatated Research 472, 1114–1122.

Halilaj, E., Rainbow, M.J., Got, C.J., Moore, D.C., Crisco, J.J., 2013. A thumb carpometacarpal joint coordinate system based on articular surface geometry. Journal of Biomechanics 46, 1031–1034.

Harmand, S., Lewis, J.E., Feibel, C.S., Lepre, C.J., Prat, S., Lenoble, A., Boes, X., Quinn, R.L., Brenet, M., Arroyo, A., Taylor, N., Clement, S., Daver, G., Brugal, J.P., Leakey, L., Mortlock, R.A., Wright, J.D., Lokorodi, S., Kirwa, C., Kent, D.V., Roche, H., 2015. 3.3-million-year-old stone tools from Lomekwi 3, West Turkana, Kenya. Nature 521, 310–315.

Hermann, M., Klein, R., 2015. A visual analytics perspective on shape analysis: State of the art and future prospects. Computers and Graphics 53, 63–71.

Hershkovitz, I., Speirs, M.S., Frayer, D., Nadel, D., Wish-Baratz, S., Arensburg, B., 1995. Ohalo II H2: a 19,000-year-old skeleton from a water-logged site at the Sea of Galilee, Israel. American Journal of Physical Anthropology 96, 215–234.

Hicks, M., Hicks, A., 2001. St Gregory's priory, Northgate, Canterbury: Excavations 1988-1991. Canterbury Archaeological Trust Limited, Canterbury.

Hildebrand, T., Ruegsegger, P., 1997. A new method for the model-independent assessment of thickness in three-dimensional images. Journal of Microscopy 185, 67–75.

Hopkins, W.D., 2013. Neuroanatomical asymmetries and handedness in chimpanzees (Pan troglodytes): a case for continuity in the evolution of hemispheric specialization. Annals of the New York Academy of Sciences 1288, 17–35.

Hopkins, W.D., Phillips, K.A., Bania, A., Calcutt, S.E., Gardner, M., Russell, J., Schaeffer, J., Lonsdorf, E.V., Ross, S.R., Schapiro, S.J., 2011. Hand preferences for coordinated bimanual actions in 777 great apes: implications for the evolution of handedness in hominins. Journal of Human Evolution 60, 605–611.

Hopkins, W.D., Russell, J., Freeman, H., Buehler, N., Reynolds, E., Schapiro, S.J., 2005. The distribution and development of handedness for manual gestures in captive chimpanzees (*Pan troglodytes*). Psychological Science 16, 487–493.

Höppner, H., Grosse-Dunker, M., Stillfried, G., Bayer, J., van der Smagt, P., 2017. Key insights into hand biomechanics: human grip stiffness can be decoupled from force by cocontraction and predicted from electromyography. Frontiers in Neurorobotics 11, 1–17.

Höppner, H., McIntyre, J., van der Smagt, P., 2013. Task dependency of grip stiffness—a study of human grip force and grip stiffness dependency during two different tasks with same grip forces. PLoS One 8, e80889.

Hu, D., Howard, D., Ren, L., 2014. Biomechanical analysis of the human finger extensor mechanism during isometric pressing. PLoS One 9, e94533.

Hunt, K.D., 1991. Mechanical implications of chimpanzee positional behavior. American Journal of Physical Anthropology 86, 521–536.

Iwasaki, N., Genda, E., Minami, A., Kaneda, K., Chao, E.Y.S., 1998. Force transmission through the wrist joint in Kienböck's disease: A two-dimensional theoretical study. Journal of Hand Surgery 23, 415–424.

Jones, F.W., 1916. Arboreal Man. Longmans Green and Co., London.

Joshi, A.A., Leahy, R.M., Badawi, R.D., Chaudhari, A.J., 2016. Registration-based morphometry for shape analysis of the bones of the human wrist. IEEE Transactions on Medical Imaging 35, 416–426.

Karakostis, F.A., Hotz, G., Scherf, H., Wahl, J., Harvati, K., 2017. Occupational manual activity is reflected on the patterns among hand entheses. American Journal of Physical Anthropology 164, 30–40.

Karakostis, F.A., Lorenzo, C., 2016. Morphometric patterns among the 3D surface areas of human hand entheses. American Journal of Physical Anthropology 160, 694–707.

Kargov, A., Pylatiuk, C., Martin, J., Schulz, S., Doderlein, L., 2004. A comparison of the grip force distribution in natural hands and in prosthetic hands. Disability and Rehabilitation 26, 705–711.

Keaveny, T.M., Morgan, E.F., Niebur, G.L., Yeh, O.C., 2001. Biomechanics of trabecular bone. Annual Review of Biomedical Engineering 3, 307–333.

Kerkhof, F.D., Brugman, E., D'Agostino, P., Dourthe, B., van Lenthe, G.H., Stockmans, F., Jonkers, I., Vereecke, E.E., 2016. Quantifying thumb opposition kinematics using dynamic computed tomography. Journal of Biomechanics 49, 1994–1999.

Key, A.J., 2016. Manual loading distribution during carrying behaviors: implications for the evolution of the hominin hand. PLoS One 11, e0163801.

Key, A.J., Dunmore, C.J., 2015. The evolution of the hominin thumb and the influence exerted by the non-dominant hand during stone tool production. Journal of Human Evolution 78, 60–69.

Key, A., Dunmore, C.J., Hatala, K.G., Williams-Hatala, E.M., 2017. Flake morphology as a record of manual pressure during stone tool production. Journal of Archaeological Science: Reports 12, 43–53.

Key, A.J.M., Lycett, S.J., 2011. Technology based evolution? A biometric test of the effects of handsize versus tool form on efficiency in an experimental cutting task. Journal of Archaeological Science 38, 1663–1670.

Key, A.J.M., Lycett, S.J., 2016. Investigating interrelationships between Lower Palaeolithic stone tool effectiveness and tool user biometric variation: implications for technological and evolutionary changes. Archaeological and Anthropological Sciences. https://doi.org/10.1007/s12520-016-0433-x

Kivell, T.L., Barros, A.P., Smaers, J.B., 2013. Different evolutionary pathways underlie the morphology of wrist bones in hominoids. BMC Evolutionary Biololgy 13, 229.

Kivell, T.L., Deane, A.S., Tocheri, M.W., Orr, C.M., Schmid, P., Hawks, J., Berger, L.R., Churchill, S.E., 2015. The hand of *Homo naledi*. Nature Communications 6, 8431.

Kivell, T.L., Kibii, J.M., Churchill, S.E., Schmid, P., Berger, L.R., 2011a. Australopithecus sediba hand demonstrates mosaic evolution of locomotor and manipulative abilities. Science 333, 1411–1417.

Kivell, T.L., Skinner, M.M., Lazenby, R., Hublin, J.J., 2011b. Methodological considerations for analyzing trabecular architecture: an example from the primate hand. Journal of Anatomy 218, 209–225.

Ladd, A.L., Crisco, J.J., Hagert, E., Rose, J., Weiss, A.P., 2014. The 2014 ABJS Nicolas Andry Award: The puzzle of the thumb: mobility, stability, and demands in opposition. Clinical Orthopaedics and Relatated Research 472, 3605–3622.

Lambers, F.M., Koch, K., Kuhn, G., Ruffoni, D., Weigt, C., Schulte, F.A., Muller, R., 2013. Trabecular bone adapts to long-term cyclic loading by increasing stiffness and normalization of dynamic morphometric rates. Bone 55, 325–334.

Landsmeer, J.M., 1955. Anatomical and functional investigations on the articulation of the human fingers. Acta Anatomica Supplementum 25, 1–69.

Landsmeer, J.M., 1962. Power grip and precision handling. Annals of the Rheumatic Diseases 21, 164–170.

Landsmeer, J.M., Long, C., 1965. The mechanism of finger control, based on electromyograms and location analysis. Acta Anatomica 60, 330–347.

Lanyon, L., Rubin, C., 1985. Functional adaptation in skeletal structures. In: Hildebrand, M., Bramble, D.M., Liem, K.F., Wake, D.B. (Eds.), Functional Vertebrate Morphology. Belknap, Cambridge, pp. 1–25.

Latypova, A., Pioletti, D.P., Terrier, A., 2017. Importance of trabecular anisotropy in finite element predictions of patellar strain after total knee arthroplasty. Medical Engineering and Physics 39, 102–105.

Lazenby, R.A., Angus, S., Cooper, D.M., Hallgrimsson, B., 2008a. A three-dimensional microcomputed tomographic study of site-specific variation in trabecular microarchitecture in the human second metacarpal. Journal of Anatomy 213, 698–705.

Lazenby, R.A., Cooper, D.M., Angus, S., Hallgrimsson, B., 2008b. Articular constraint, handedness, and directional asymmetry in the human second metacarpal. Journal of Human Evolution 54, 875–885.

Lazenby, R.A., Skinner, M.M., Hublin, J.J., Boesch, C., 2011a. Metacarpal trabecular architecture variation in the chimpanzee (*Pan troglodytes*): Evidence for locomotion and tool-use? American Journal of Physical Anthropology 144, 215–225.

Lazenby, R.A., Skinner, M.M., Kivell, T.L., Hublin, J.J., 2011b. Scaling VOI size in 3D muCT studies of trabecular bone: a test of the over-sampling hypothesis. American Journal of Physical Anthropology 144, 196–203.

Lazic, S.E., 2010. The problem of pseudoreplication in neuroscientific studies: is it affecting your analysis? BMC Neuroscience 11, 5.

Leakey, L.S., Tobias, P.V., Napier, J.R., 1964. A New Species of the Genus *Homo* from Olduvai Gorge. Nature 202, 7–9.

Lee, A.T., Williams, A.A., Lee, J., Cheng, R., Lindsey, D.P., Ladd, A.L., 2013. Trapezium trabecular morphology in carpometacarpal arthritis. Journal of Hand Surgery 38, 309–315.

Lemelin, P., Schmitt, D., 2016. On primitiveness, prehensility, and opposability of the primate hand: the contributions of Frederic Wood Jones and John Russell Napier. In: Kivell, T.L., Lemelin, P., Richmond, B.G., Schmitt, D. (Eds.), The Evolution of the Primate Hand. Springer, New York, pp. 5–13.

Leventhal, E.L., Moore, D.C., Akelman, E., Wolfe, S.W., Crisco, J.J., 2010. Carpal and forearm kinematics during a simulated hammering task. Journal of Hand Surgery 35, 1097–1104.

Lewis, O.J., 1969. The hominoid wrist joint. American Journal of Physical Anthropology 30, 251–267.

Liu, M.J., Xiong, C.H., Hu, D., 2016a. Assessing the manipulative potentials of monkeys, apes and humans from hand proportions: implications for hand evolution. Proceedings of the Royal Society B 283, 20161923.

Liu, Y., Jiang, L., Yang, D., Liu, H., 2016b. Analysis of Hand and Wrist Postural Synergies in Tolerance Grasping of Various Objects. PLoS One 11, e0161772.

Lorenzo, C., Arsuaga, J.L., Carretero, J.M., 1999. Hand and foot remains from the Gran Dolina Early Pleistocene site (Sierra de Atapuerca, Spain). Journal of Human Evolution 37, 501–522.

Lorenzo, C., Pablos, A., Carretero, J.M., Huguet, R., Valverdú, J., Martinón-Torres, M., Arsuaga, J.L., Carbonell, E., Bermúdez de Castro, J.M., 2015. Early Pleistocene human hand phalanx from the Sima del Elefante (TE) cave site in Sierra de Atapuerca (Spain). Journal of Human Evolution 78, 114–121.

Macintosh, A.A., Pinhasi, R., Stock, J.T., 2014. Divergence in male and female manipulative behaviors with the intensification of metallurgy in Central Europe. PLoS One 9, e112116.

Macintosh, A.A., Pinhasi, R., Stock, J.T., 2017. Prehistoric women's manual labor exceeded that of athletes through the first 5500 years of farming in Central Europe. Science Advances 3, eaao3893.

Majima, M., Horii, E., Matsuki, H., Hirata, H., Genda, E., 2008. Load transmission through the wrist in the extended position. Journal of Hand Surgery 33, 182–188.

Maki, J., Trinkaus, E., 2011. Opponens pollicis mechanical effectiveness in neandertals and early modern humans. PaleoAnthropology 2011, 62–71.

Maquer, G., Musy, S.N., Wandel, J., Gross, T., Zysset, P.K., 2015. Bone volume fraction and fabric anisotropy are better determinants of trabecular bone stiffness than other morphological variables. Journal of Bone and Mineral Research 30, 1000–1008.

Marangoni, A., Belli, L.M., Caramelli, D., Jacopo, M.C., Zavattaro, M., Manzi, G., 2011. The Tierra del Fuego, its ancient inhabitants, and the collections of human skeletal remains in the Museums of Anthropology of Florence and Rome. Museological significance, past researches, perspectives. Museologia Scientifica 5, 88–96.

Marchi, D., 2005. The cross-sectional geometry of the hand and foot bones of the hominoidea and its relationship to locomotor behavior. Journal of Human Evolution 49, 743–761.

Marchi, D., Shaw, C.N., 2011. Variation in fibular robusticity reflects variation in mobility patterns. Journal of Human Evolution 61, 609–616.

Márquez-Florez, K., Vergara-Amador, E., de Las Casas, E.B., Garzón-Alvarado, D.A., 2015. Theoretical distribution of load in the radius and ulna carpal joint. Computers in Biology and Medicine 60, 100–106.

Marzke, M.W., 1983. Joint functions and grips of the *Australopithecus afarensis* hand, with special reference to the region of the capitate. Journal of Human Evolution 12, 197–211.

Marzke, M.W., 1997. Precision grips, hand morphology, and tools. American Journal of Physical Anthropology 102, 91–110.

Marzke, M.W., 2013. Tool making, hand morphology and fossil hominins. Philosophical Transactions of the Royal Society B 368, 20120414.

Marzke, M.W., Marchant, L.F., McGrew, W.C., Reece, S.P., 2015. Grips and hand movements of chimpanzees during feeding in Mahale Mountains National Park, Tanzania. American Journal of Physical Anthropology 156, 317–326.

Marzke, M.W., Tocheri, M.W., Steinberg, B., Femiani, J.D., Reece, S.P., Linscheid, R.L., Orr, C.M., Marzke, R.F., 2010. Comparative 3D quantitative analyses of trapeziometacarpal joint surface curvatures among living catarrhines and fossil hominins. American Journal of Physical Anthropology 141, 38–51.

Marzke, M.W., Toth, N., Schick, K., Reece, S., Steinberg, B., Hunt, K., Linscheid, R.L., An, K.N., 1998. EMG study of hand muscle recruitment during hard hammer percussion manufacture of Oldowan tools. American Journal of Physical Anthropology 105, 315–332.

Marzke, M.W., Wullstein, K.L., 1996. Chimpanzee and human grips: A new classification with a focus on evolutionary morphology. International Journal of Primatology 17, 117–139.

Marzke, M.W., Wullstein, K.L., Viegas, S.F., 1992. Evolution of the power ("squeeze") grip and its morphological correlates in hominids. American Journal of Physical Anthropology 89, 283–298.

Matarazzo, S.A., 2015. Trabecular architecture of the manual elements reflects locomotor patterns in primates. PLoS One 10, e0120436.

Mittnik, A., Wang, C.C., Svoboda, J., Krause, J., 2016. A molecular approach to the sexing of the triple burial at the upper paleolithic site of Dolní Věstonice. PLoS One 11, e0163019.

Moojen, T.M., Snel, J.G., Ritt, M.J., Kauer, J.M., Venema, H.W., Bos, K.E., 2002a. Three-dimensional carpal kinematics in vivo. Clinical Biomechanics 17, 506–514.

Moojen, T.M., Snel, J.G., Ritt, M.J., Venema, H.W., Kauer, J.M., Bos, K.E., 2002b. Scaphoid kinematics in vivo. Journal of Hand Surgery 27, 1003–1010.

Musgrave, J.H., 1971. How dextrous was neanderthal man? Nature 233, 538–541.

Napier, J., 1962. Fossil hand bones from Olduvai Gorge. Nature 196, 409–411.

Napier, J.R., 1956. The prehensile movements of the human hand. Journal of Bone and Joint Surgery, British Volume 38-B, 902–913.

Napier, J.R., 1960. Studies of the hands of living primates. Proceedings of the Zoological Society of London 134, 647–657.

Neufuss, J., Humle, T., Cremaschi, A., Kivell, T.L., 2017. Nut-cracking behavior in wild-born, rehabilitated bonobos (*Pan paniscus*): a comprehensive study of hand-preference, hand grips and efficiency. American Journal of Primatology 79, 1–16.

Niewoehner, W.A., 2001. Behavioral inferences from the Skhul/Qafzeh early modern human hand remains. Proceedings of the National Academy of Sciences USA 98, 2979–2984.

Niewoehner, W., 2006. Neanderthal hands in their proper perspective. In: Harvati, K., Harrison, T. (Eds.), Neanderthals Revisited: New Approaches and Perspectives, 2nd ed. Springer, Dordrecht, pp. 157–190.

Niewoehner, W.A., Bergstrom, A., Eichele, D., Zuroff, M., Clark, J.T., 2003. Digital analysis: manual dexterity in Neanderthals. Nature 422, 395.

Nufer, P., Goldhahn, J., Kohler, T., Kuhn, V., Muller, R., Herren, D.B., 2008. Microstructural adaptation in trapezial bone due to subluxation of the thumb. Journal of Orthopaedic Research 26, 208–216.

Orr, C.M., 2017. Locomotor hand postures, carpal kinematics during wrist extension, and associated morphology in anthropoid primates. Anatomical Record 300, 382–401.

Orr, C.M., 2018. Kinematics of the anthropoid os centrale and the functional consequences of scaphoid-centrale fusion in African apes and hominins. Journal of Human Evolution 114, 102–117.

Orr, C.M., Leventhal, E.L., Chivers, S.F., Marzke, M.W., Wolfe, S.W., Crisco, J.J., 2010. Studying primate carpal kinematics in three dimensions using a computed-tomography-based markerless registration method. Anatomical Record 293, 692–709.

Ozcivici, E., Judex, S., 2014. Trabecular bone recovers from mechanical unloading primarily by restoring its mechanical function rather than its morphology. Bone 67, 122–129.

Pahr, D.H., Zysset, P.K., 2009a. A comparison of enhanced continuum FE with micro FE models of human vertebral bodies. Journal of Biomechanics 42, 455–462.

Pahr, D.H., Zysset, P.K., 2009b. From high-resolution CT data to finite element models: development of an integrated modular framework. Computer Methods in Biomechanics and Biomedical Engineering 12, 45–57.

Pahr, D.H., Zysset, P.K., 2016. Finite element-based mechanical assessment of bone quality on the basis of in vivo images. Current Osteoporosis Reports 14, 374–385.

Paoli, G., Borgognini Tarli, S.M., Klir, P., Strouhal, E., Tofanelli, S., Del Santo Valli, M.T., Pavelcova, B., 1993. Paleoserology of the Christian population at Sayala (Lower Nubia): an evaluation of the reliability of the results. American Journal of Physical Anthropology 92, 263–272.

Pataky, T.C., Slota, G.P., Latash, M.L., Zatsiorsky, V.M., 2012. Radial force distribution changes associated with tangential force production in cylindrical grasping, and the importance of anatomical registration. Journal of Biomechanics 45, 218–224.

Patel, B.A., Carlson, K.J., 2007. Bone density spatial patterns in the distal radius reflect habitual hand postures adopted by quadrupedal primates. Journal of Human Evolution 52, 130–141.

Pearson, O.M., Sparacello, V.S., 2017. Behavioral differences between near eastern neanderthals and the early modern humans from Skhul and Qafzeh: an assessment based on comparative samples of Holocene humans. In: Marom, A., Hovers, E. (Eds.), Human Paleontology and Prehistory. Springer International Publishing, Cham, pp. 175–186.

Perchalski, B., Placke, A., Sukhdeo, S.M., Shaw, C.N., Gosman, J.H., Raichlen, D.A., Ryan, T.M., 2017. Asymmetry in the cortical and trabecular bone of the human humerus during development. Anatomical Record. https://doi.org/10.1002/ar.23705

Phillips, A.T.M., Villette, C.C., Modenese, L., 2015. Femoral bone mesoscale structural architecture prediction using musculoskeletal and finite element modelling. International Biomechanics 2, 43–61.

Polk, J.D., 2002. Adaptive and phylogenetic influences on musculoskeletal design in cercopithecine primates. Journal of Experimental Biology 205, 3399–3412.

Pontzer, H., Lieberman, D.E., Momin, E., Devlin, M.J., Polk, J.D., Hallgrimsson, B., Cooper, D.M., 2006. Trabecular bone in the bird knee responds with high sensitivity to changes in load orientation. Journal of Experimental Biology 209, 57–65.

Poole, K.E., Treece, G.M., Mayhew, P.M., Vaculik, J., Dungl, P., Horak, M., Stepan, J.J., Gee, A.H., 2012. Cortical thickness mapping to identify focal osteoporosis in patients with hip fracture. PLoS One 7, e38466.

Pouydebat, E., Gorce, P., Coppens, Y., Bels, V., 2009. Biomechanical study of grasping according to the volume of the object: human versus non-human primates. Journal of Biomechanics 42, 266–272.

Pouydebat, E., Fragaszy, D., Kivell, T.L., 2014. Grasping in primates: for feeding, moving and human specificities. Bulletins et Mémoires de la Société d'Anthropologie de Paris, 26, 129–133.

Pouydebat, E., Reghem, E., Borel, A., Gorce, P., 2011. Diversity of grip in adults and young humans and chimpanzees (*Pan troglodytes*). Behavioural Brain Research 218, 21–28.

Proffitt, T., Luncz, L.V., Falotico, T., Ottoni, E.B., de la Torre, I., Haslam, M., 2016. Wild monkeys flake stone tools. Nature 539, 85–88.

Putt, S.S., Wijeakumar, S., Franciscus, R.G., Spencer, J.P., 2017. The functional brain networks that underlie Early Stone Age tool manufacture. Nature Human Behaviour 1, 0102.

Python 3.6, 2017. Python programming language. Python Software Foundation, Beaverton.

Qiu, D., Kamper, D.G., 2014. Orthopaedic applications of a validated force-based biomechanical model of the index finger. In: 36th Annual International Conference of the IEEE Engineering in Medicine and Biology Society. IEEE, Chicago, pp. 4013–4016.

R Core Team, 2017. R: A language and environment for statistical computing. R Foundation for Statistical Computing, Vienna.

Rabey, K.N., Green, D.J., Taylor, A.B., Begun, D.R., Richmond, B.G., McFarlin, S.C., 2015. Locomotor activity influences muscle architecture and bone growth but not muscle attachment site morphology. Journal of Human Evolution 78, 91–102.

Rafferty, K.L., Ruff, C.B., 1994. Articular structure and function in *Hylobates*, *Colobus*, and *Papio*. American Journal of Physical Anthropology 94, 395–408.

Rainbow, M.J., Kamal, R.N., Leventhal, E., Akelman, E., Moore, D.C., Wolfe, S.W., Crisco, J.J., 2013. In vivo kinematics of the scaphoid, lunate, capitate, and third metacarpal in extreme wrist flexion and extension. Journal of Hand Surgery 38, 278–288.

Rainbow, M.J., Kamal, R.N., Moore, D.C., Akelman, E., Wolfe, S.W., Crisco, J.J., 2015. Subject-specific carpal ligament elongation in extreme positions, grip, and the dart thrower's motion. Journal of Biomechanical Engineering 137, 111006.

Rainbow, M.J., Wolff, A.L., Crisco, J.J., Wolfe, S.W., 2016. Functional kinematics of the wrist. Journal of Hand Surgery Europe 41, 7–21.

Reina, N., Cavaignac, E., Trousdale, W.H., Laffosse, J.M., Braga, J., 2017. Laterality and grip strength influence hand bone micro-architecture in modern humans, an HRpQCT study. Journal of Anatomy 230, 796–804.

Reznikov, N., Chase, H., Brumfeld, V., Shahar, R., Weiner, S., 2015. The 3D structure of the collagen fibril network in human trabecular bone: relation to trabecular organization. Bone 71, 189–195.

Reznikov, N., Phillips, C., Cooke, M., Garbout, A., Ahmed, F., Stevens, M.M., 2017. Functional adaptation of the calcaneus in historical foot binding. Journal of Bone and Mineral Research 32, 1915–1925.

Rhodes, J.A., Knusel, C.J., 2005. Activity-related skeletal change in medieval humeri: cross-sectional and architectural alterations. American Journal of Physical Anthropology 128, 536–546.

Ricklan, D.E., 1987. Functional anatomy of the hand of *Australopithecus africanus*. Journal of Human Evolution 16, 643–664.

Ritter, Z., Belavy, D., Baumann, W.W., Felsenberg, D., 2017. In vivo bone modeling rates determination and compressive stiffness variations before, during 60 days bed rest and two years follow up: A micro-FE-analysis from HR-pQCT measurements of the berlin Bed Rest Study-2. Acta Astronautica 132, 67–77.

Roberts, T.J., Konow, N., 2013. How tendons buffer energy dissipation by muscle. Exercise and Sport Sciences Reviews 41, 186–193.

Rolian, C., 2016. The role of genes and development in the evolution of the primate hand. In: Kivell, T.L., Lemelin, P., Richmond, B.G., Schmitt, D. (Eds.), The Evolution of the Primate Hand. Springer, New York, pp. 101–130.

Rolian, C., Lieberman, D.E., Hallgrimsson, B., 2010. The coevolution of human hands and feet. Evolution 64, 1558–1568.

Rolian, C., Lieberman, D.E., Zermeno, J.P., 2011. Hand biomechanics during simulated stone tool use. Journal of Human Evolution 61, 26–41.

Ruff, C.B., 2002. Long bone articular and diaphyseal structure in old world monkeys and apes. I: locomotor effects. American Journal of Physical Anthropology 119, 305–342.

Ruff, C., Holt, B., Trinkaus, E., 2006. Who’s afraid of the big bad Wolff?: “Wolff's law” and bone functional adaptation. American Journal of Physical Anthropology 129, 484-498.

Ryan, T.M., Ketcham, R.A., 2002. Femoral head trabecular bone structure in two omomyid primates. Journal of Human Evolution 43, 241–263.

Ryan, T.M., Shaw, C.N., 2012. Unique suites of trabecular bone features characterize locomotor behavior in human and non-human anthropoid primates. PLoS One 7, e41037.

Ryan, T.M., Shaw, C.N., 2013. Trabecular bone microstructure scales allometrically in the primate humerus and femur. Proceedings of the Royal Society B: Biological Sciences 280, 20130172.

Ryan, T.M., Shaw, C.N., 2015. Gracility of the modern *Homo sapiens* skeleton is the result of decreased biomechanical loading. Proceedings of the National Academy of Sciences of the United States of America 112, 372–377.

Ryan, T.M., Raichlen, D.A., Gosman, J.H., 2017. Structural and mechanical changes in trabecular bone during early development in the human femur and humerus. In: Percival, C.J., Richtsmeier, J.T. (Eds.), Building Bones: Bone Formation and Development in Anthropology. Cambridge University Press, Cambridge, pp. 281–302.

Saffar, R.A.A., 2016. Quantification of variable palmar ligaments around the triquetrum-hamate joint determined by lunate type. Ph.D. Dissertation, University of Glasgow.

Scherf, H., Tilgner, R., 2009. A new high-resolution computed tomography (CT) segmentation method for trabecular bone architectural analysis. American Journal of Physical Anthropology 140, 39–51.

Scherf, H., Wahl, J., Hublin, J.J., Harvati, K., 2016. Patterns of activity adaptation in humeral trabecular bone in Neolithic humans and present-day people. American Journal of Physical Anthropology 159, 106–115.

Schilling, A.M., Tofanelli, S., Hublin, J.J., Kivell, T.L., 2014. Trabecular bone structure in the primate wrist. Journal of Morphology 275, 572–585.

Schlecht, S.H., Bigelow, E.M., Jepsen, K.J., 2014. Mapping the natural variation in whole bone stiffness and strength across skeletal sites. Bone 67, 15–22.

Schmid, P., Berger, L.R., 1997. Middle Pleistocene hominid carpal proximal phalanx from the Gladysvale site, South Africa. South African Journal of Science 93, 430–431.

Schneider, M.T.Y., Zhang, J., Crisco, J.J., Weiss, A.C., Ladd, A.L., Mithraratne, K., Nielsen, P., Besier, T., 2017. Trapeziometacarpal joint contact varies between men and women during three isometric functional tasks. Medical Engineering & Physics 50, 43–49.

Schulte, F.A., Lambers, F.M., Kuhn, G., Muller, R., 2011. In vivo micro-computed tomography allows direct three-dimensional quantification of both bone formation and bone resorption parameters using time-lapsed imaging. Bone 48, 433–442.

Schulte, F.A., Ruffoni, D., Lambers, F.M., Christen, D., Webster, D.J., Kuhn, G., Muller, R., 2013. Local mechanical stimuli regulate bone formation and resorption in mice at the tissue level. PLoS One 8, e62172.

Shaw, C.N., Hofmann, C.L., Petraglia, M.D., Stock, J.T., Gottschall, J.S., 2012. Neandertal humeri may reflect adaptation to scraping tasks, but not spear thrusting. PLoS One 7, e40349.

Schwarcz, H.P., Grün, R., Vandermeersch, B., Bar-Yosef, O., Valladas, H., Tchernov, E., 1988. ESR dates for the hominid burial site of Qafzeh in Israel. Journal of Human Evolution 17, 733–737.

Schwiedrzik, J., Gross, T., Bina, M., Pretterklieber, M., Zysset, P., Pahr, D., 2016. Experimental validation of a nonlinear muFE model based on cohesive-frictional plasticity for trabecular bone. International Journal for Numerical Methods in Biomedical Engineering 32, e02739.

Shrewsbury, M.M., Marzke, M.W., Linscheid, R.L., Reece, S.P., 2003. Comparative morphology of the pollical distal phalanx. American Journal of Physical Anthropology 121, 30–47.

Singh, M., Nagrath, A.R., Maini, P.S., 1970. Changes in trabecular pattern of the upper end of the femur as an index of osteoporosis. Journal of Bone and Joint Surgery 52, 457–467.

Skinner, M.M., Stephens, N.B., Tsegai, Z.J., Foote, A.C., Nguyen, N.H., Gross, T., Pahr, D.H., Hublin, J.J., Kivell, T.L., 2015a. Human-like hand use in *Australopithecus africanus*. Science 347, 395–399.

Skinner, M.M., Stephens, N.B., Tsegai, Z.J., Foote, A.C., Nguyen, N.H., Gross, T., Pahr, D.H., Hublin, J.J., Kivell, T.L., 2015b. Response to comment on "Human-like hand use in *Australopithecus africanus*". Science 348, 1101.

Sládek, V., Hora, M., Farkašová, K., Rocek, T.R., 2016. Impact of grinding technology on bilateral asymmetry in muscle activity of the upper limb. Journal of Archaeological Science 72, 142–156.

Sládek, V., Trinkaus, E., Hillson, S.W., Holliday, T.W., 2000. The People of the Pavlovian: Skeletal Catalogue and Osteometrics of the Gravettian Fossil Hominids from Dolní Věstonice and Pavlov. Academy of Sciences of the Czech Republic, Institute of Archaeology, Brno, Dolní Věstonice.

Smith, L.M., Bigelow, E.M., Nolan, B.T., Faillace, M.E., Nadeau, J.H., Jepsen, K.J., 2014. Genetic perturbations that impair functional trait interactions lead to reduced bone strength and increased fragility in mice. Bone 67, 130–138.

Sparacello, V., Pettitt, P.B., Roberts, C., 2015. Funerary dynamics of an Epipalaeolithic cemetery: a new database on Arene Candide skeletal remains. Proceedings of the European Society for the Study of Human Evolution 4, 209.

Stephens, N.B., Kivell, T.L., Pahr, D.H., Hublin, J.J., Skinner, M.M., 2015. Visualising trabecular bone architecture and distribution in the human hand: variation, consistency, and implications for reconstructing behaviour. Proceedings of the European Society for the Study of Human Evolution 4, 211.

Stephens, N.B., Kivell, T.L., Gross, T., Pahr, D.H., Lazenby, R.A., Hublin, J.J., Hershkovitz, I., Skinner, M.M., 2016a. Trabecular architecture in the thumb of *Pan* and *Homo*: implications for investigating hand use, loading, and hand preference in the fossil record. American Journal of Physical Anthropology 161, 603–619.

Stephens, N.B., Kivell, T.L., Pahr, D.H., Gee, A.H., Treece, G.M., Hublin, J.J., Skinner, M.M., 2016b. Signals of loading and function in the human hand: a multi-method analysis of the external cortical and internal trabecular bone of the metacarpals. American Journal of Physical Anthropology 159 S62, 302–303.

Stieglitz, J., Trumble, B.C., Kaplan, H., Gurven, M., 2017. Horticultural activity predicts later localized limb status in a contemporary pre-industrial sample. American Journal of Physical Anthropology 163, 425–436.

Stock, J.T., 2006. Hunter-gatherer postcranial robusticity relative to patterns of mobility, climatic adaptation, and selection for tissue economy. American Journal of Physical Anthropology 131, 194–204.

Stock, J.T., Shirley, M.K., Sarringhaus, L.A., Davies, T.G., Shaw, C.N., 2013. Skeletal evidence for variable patterns of handedness in chimpanzees, human hunter-gatherers, and recent British populations. Annals of the New York Academy of Sciences 1288, 86–99.

Stratford, D., Heaton, J.L., Pickering, T.R., Caruana, M.V., Shadrach, K., 2016. First hominin fossils from Milner Hall, Sterkfontein, South Africa. Journal of Human Evolution 91, 167–173.

Strauss, A., Oliveira, R.E., Bernardo, D.V., Salazar-Garcia, D.C., Talamo, S., Jaouen, K., Hubbe, M., Black, S., Wilkinson, C., Richards, M.P., Araujo, A.G., Kipnis, R., Neves, W.A., 2015. The oldest case of decapitation in the new world (Lapa do Santo, east-central Brazil). PLoS One 10, e0137456.

Strouhal, E., Jungwirth, J., 1979. Paleogenetics of the late Roman-early Byzantine cemeteries at Sayala, Egyptian Nubia. Journal of Human Evolution 8, 699–703.

Su, A., Carlson, K.J., 2017. Comparative analysis of trabecular bone structure and orientation in South African hominin tali. Journal of Human Evolution 106, 1–18.

Su, A., Wallace, I.J., Nakatsukasa, M., 2013. Trabecular bone anisotropy and orientation in an early Pleistocene hominin talus from East Turkana, Kenya. Journal of Human Evolution 64, 667–677.

Sugiyama, T., Price, J.S., Lanyon, L.E., 2010. Functional adaptation to mechanical loading in both cortical and cancellous bone is controlled locally and is confined to the loaded bones. Bone 46, 314–321.

Susman, R.L., 1979. Comparative and functional morphology of hominoid fingers. American Journal of Physical Anthropology 50, 215–236.

Susman, R.L., 1991. Who made the oldowan tools? Fossil evidence for tool behavior in Plio-Pleistocene hominids. Journal of Anthropological Research 47, 129–151.

Susman, R.L., 1994. Fossil evidence for early hominid tool use. Science 265, 1570–1573.

Susman, R.L., 1998. Hand function and tool behavior in early hominids. Journal of Human Evolution 35, 23–46.

Sylvester, A.D., Terhune, C.E., 2017. Trabecular mapping: Leveraging geometric morphometrics for analyses of trabecular structure. American Journal of Physical Anthropology 163, 553–569.

Synek, A., Pahr, D.H., 2016. The effect of the extensor mechanism on maximum isometric fingertip forces: A numerical study on the index finger. Journal of Biomechanics 49, 3423–3429.

Taghizadeh, E., Chandran, V., Reyes, M., Zysset, P., Buchler, P., 2017. Statistical analysis of the inter-individual variations of the bone shape, volume fraction and fabric and their correlations in the proximal femur. Bone 103, 252–261.

Tocheri, M.W., Marzke, M.W., Liu, D., Bae, M., Jones, G.P., Williams, R.C., Razdan, A., 2003. Functional capabilities of modern and fossil hominid hands: three-dimensional analysis of trapezia. American Journal of Physical Anthropology 122, 101–112.

Tocheri, M.W., Orr, C.M., Jacofsky, M.C., Marzke, M.W., 2008. The evolutionary history of the hominin hand since the last common ancestor of *Pan* and *Homo*. Journal of Anatomy 212, 544–562.

Tocheri, M.W., Razdan, A., Williams, R.C., Marzke, M.W., 2005. A 3D quantitative comparison of trapezium and trapezoid relative articular and nonarticular surface areas in modern humans and great apes. Journal of Human Evolution 49, 570–586.

Tommasini, S.M., Hu, B., Nadeau, J.H., Jepsen, K.J., 2009. Phenotypic integration among trabecular and cortical bone traits establishes mechanical functionality of inbred mouse vertebrae. Journal of Bone and Mineral Research 24, 606–620.

Trinkaus, E., 1989. Olduvai Hominid 7 trapezial metacarpal 1 articular morphology: contrasts with recent humans. American Journal of Physical Anthropology 80, 411–416.

Trinkaus, E., Churchill, S.E., Ruff, C.B., 1994. Postcranial robusticity in Homo. II: Humeral bilateral asymmetry and bone plasticity. American Journal of Physical Anthropology 93, 1–34.

Trinkaus, E., 2016. The evolution of the hand in Pleistocene *Homo*. In: Kivell, T.L., Lemelin, P., Richmond, B.G., Schmitt, D. (Eds.), The Evolution of the Primate Hand. Springer, New York, pp. 545–571.

Trinkaus, E., Formicola, V., Svoboda, J., Hillson, S.W., Holliday, T.W., 2001. Dolní Věstonice 15: pathology and persistence in the Pavlovian. Journal of Archaeological Science 28, 1291–1308.

Tsegai, Z.J., Kivell, T.L., Gross, T., Nguyen, N.H., Pahr, D.H., Smaers, J.B., Skinner, M.M., 2013. Trabecular bone structure correlates with hand posture and use in hominoids. PLoS One 8, e78781.

Tsegai, Z.J., Stephens, N.B., Treece, G.M., Skinner, M.M., Kivell, T.L., Gee, A.H., 2017. Cortical bone mapping: an application to hand and foot bones in hominoids. Comptes Rendus Palevol 16, 690–701.

Tsegai, Z.J., Skinner, M.M., Pahr, D.H., Hublin, J.-J., Kivell, T.L., 2018. Systemic patterns of trabecular bone across the human and chimpanzee skeleton. Journal of Anatomy. https://doi.org/10.1111/joa.12776

Varga, P., Schefzig, P., Unger, E., Mayr, W., Zysset, P.K., Erhart, J., 2013. Finite element based estimation of contact areas and pressures of the human scaphoid in various functional positions of the hand. Journal of Biomechanics 46, 984–990.

Venkataraman, V.V., Rolian, C., Gordon, A.D., Patel, B.A., 2013. A resampling approach and implications for estimating the phalangeal index from unassociated hand bones in fossil primates. American Journal of Physical Anthropology 151, 280–289.

Vereecke, E.E., Wunderlich, R.E., 2016. Experimental research on hand use and function in primates. In: Kivell, T.L., Lemelin, P., Richmond, B.G., Schmitt, D. (Eds.), The Evolution of the Primate Hand. Springer, New York, pp. 259–284.

Vergara, M., Sancho-Bru, J.L., Gracia-Ibáñez, V., Pérez-González, A., 2014. An introductory study of common grasps used by adults during performance of activities of daily living. Journal of Hand Therapy 27, 225–233.

Viaro, R., Tia, B., Coude, G., Canto, R., Oliynyk, A., Salmas, P., Masia, L., Sandini, G., Fadiga, L., 2017. Finger pressure adjustments to various object configurations during precision grip in humans and monkeys. European Journal of Neuroscience 45, 1473–1484.

Vickerton, P., Jarvis, J.C., Gallagher, J.A., Akhtar, R., Sutherland, H., Jeffery, N., 2014. Morphological and histological adaptation of muscle and bone to loading induced by repetitive activation of muscle. Proceedings of the Royal Society B 281, 20140786.

Visalberghi, E., Addessi, E., Truppa, V., Spagnoletti, N., Ottoni, E., Izar, P., Fragaszy, D., 2009. Selection of effective stone tools by wild bearded capuchin monkeys. Current Biology 19, 213–217.

Vlček, E., 1975. Morphology of the first metacarpal of neandertal individuals from the Crimea. Bulletins et Mémoires de la Société d'Anthropologie de Paris 2, 257–276.

Wallace, I.J., Middleton, K.M., Lublinsky, S., Kelly, S.A., Judex, S., Garland, T. Jr., Demes, B., 2010. Functional significance of genetic variation underlying limb bone diaphyseal structure. American Journal of Physical Anthropology 143, 21–30.

Wallace, I.J., Judex, S., Demes, B., 2015a. Effects of load-bearing exercise on skeletal structure and mechanics differ between outbred samples of mice. Bone 72, 1–8.

Wallace, I.J., Pagnotti, G.M., Rubin-Sigler, J., Naeher, M., Copes, L.E., Judex, S., Rubin, C.T., Demes, B., 2015b. Focal enhancement of the skeleton to exercise correlates with responsivity of bone marrow mesenchymal stem cells rather than peak external forces. Journal of Experimental Biology 218, 3002–3009.

Wallace, I.J., Demes, B., Judex, S., 2017a. Ontogenetic and genetic influences on bone's responsiveness to mechanical signals. In: Percival, C.J., Richtsmeier, J.T. (Eds.), Building Bones: Bone Formation and Development in Anthropology. Cambridge University Press, Cambridge, pp. 233–253.

Wallace, I.J., Winchester, J.M., Su, A., Boyer, D.M., Konow, N., 2017b. Physical activity alters limb bone structure but not entheseal morphology. Journal of Human Evolution 107, 14–18.

Ward, C.V., Tocheri, M.W., Plavcan, J.M., Brown, F.H., Manthi, F.K., 2014. Early Pleistocene third metacarpal from Kenya and the evolution of modern human-like hand morphology. Proceedings of the National Academy of Sciences USA 111, 121–124.

Washburn, S.L., 1960. Tools and human evolution. Scientific American 203, 63–75.

Waskom, M., Botvinnik, O., O’Kane, D., Hobson, P., Lukauskas, S., Gemperline, D.C., Augspurger, T., Halchenko, Y., Cole, J.B., Warmenhoven, J., Ruiter, J. de, Pye, C., Hoyer, S., Vanderplas, J., Villalba, S., Kunter, G., Quintero, E., Bachant, P., Martin, M., Meyer, K., Miles, A., Ram, Y., Yarkoni, T., Williams, M.L., Evans, C., Fitzgerald, C., Brian, Fonnesbeck, C., Lee, A., Qalieh, A.,

2017. Seaborn: statistical data visualization v0.8.0. Zenodo. https://doi.org//10.5281/zenodo.883859.

Whiten, A., Goodall, J., McGrew, W.C., Nishida, T., Reynolds, V., Sugiyama, Y., Tutin, C.E., Wrangham, R.W., Boesch, C., 1999. Cultures in chimpanzees. Nature 399, 682–685.

Williams, E.M., Gordon, A.D., Richmond, B.G., 2010. Upper limb kinematics and the role of the wrist during stone tool production. American Journal of Physical Anthropology 143, 134–145.

Williams, E.M., Gordon, A.D., Richmond, B.G., 2012. Hand pressure distribution during Oldowan stone tool production. Journal of Human Evolution 62, 520–532.

Williams, E.M., Gordon, A.D., Richmond, B.G., 2014. Biomechanical strategies for accuracy and force generation during stone tool production. Journal of Human Evolution 72, 52–63.

Williams-Hatala, E.M., Hatala, K.G., Gordon, M., Kasper, M., Kivell, T.L., 2017. The biomechanics of stone tool behaviors and implications for the evolution of the human hand. American Journal of Physical Anthropology 162, 411.

Wong, A.L., sMeals, C.G., Ruff, C.B., 2017. Computed tomographic analysis of the internal structure of the metacarpals and its impliscations for hand use, pathology, and surgical intervention. Anatomical Science International. https://doi.org/10.1007/s12565-017-0400-3.

Wood, B., 2014. Human evolution: fifty years after *Homo habilis*. Nature 508, 31–33.

Wu, J.Z., Sinsel, E.W., Zhao, K.D., An, K.N., Buczek, F.L., 2015. Analysis of the constraint joint loading in the thumb during pipetting. Journal of Biomechanical Engineering 137, 084501.

Yang, H., Embry, R.E., Main, R.P., 2017. Effects of loading duration and short rest insertion on cancellous and cortical bone adaptation in the mouse tibia. PLoS One 12, e0169519.

Young, R.W., 2003. Evolution of the human hand: the role of throwing and clubbing. Journal of Anatomy 202, 165–174.

Zeininger, A., Richmond, B.G., Hartman, G., 2011. Metacarpal head biomechanics: a comparative backscattered electron image analysis of trabecular bone mineral density in *Pan troglodytes*, *Pongo pygmaeus*, and *Homo sapiens*. Journal of Human Evolution 60, 703–710.

Zlatev, J., 2008. From proto-mimesis to language: evidence from primatology and social neuroscience. Journal of Physiology-Paris 102, 137–151.

Zysset, P.K., 2003. A review of morphology-elasticity relationships in human trabecular bone: theories and experiments. Journal of Biomechanics 36, 1469–1485.

Figure captions

Figure 1. Depiction of the linear mixed effect model setups in the study. Type 1 compares the segments (carpals, head/bases from the rays II–V), type 2 the regions of the metacarpals (head/base dorsoradial, dorsoulnar, palmoradial, palmoulnar), and type 3 the regions of the phalanges (head/base ulnar and radial). For each model type, ‘subtype a’ contains data from all the bones of the hand and ‘subtype b’ contains all data from the bones of the thumb. Bones are colored to help illustrate the different functional groups used in the linear models: hamatotrqiuetral (dark pink), capitotrapezoid (light pink), scapholunate (red-orange), thumb

group (purple), ray II (green), ray III (teal), ray IV (yellow), and ray V (orange). See text for a more detailed description.

Figure 2. Comparison of post-Neolithic and forager mean segment values. Values of BV/TV, E, and DA are all mapped onto right hands. Here the differences in the carpals and the heads of the phalanges are most obvious for BV/TV and E. Also note the extremely low DA in the carpals of the forager sample. The data pictured here pertains to model type 1.

Figure 3. Comparison of post-Neolithic and forager average Tb.Th (mm) and Tb.Sp (mm) by bone segment. Here the Tb.Sp is nearly identical between the two, with the Tb.Th differing in the carpals, metacarpal bases, and the heads of the phalanges.

Figure 4. Violin plots of each carpal bone for BV/TV, E, and DA, which show each individual value (horizontal black bars, with width defined by counts per bin) as well as the distribution by group (outer curve, defined by width multiplied by kernel of 2 standard deviations). The post-Neolithic sample is indicated by the lighter shades to the left of the vertical mid-bar, while the forager sample is indicated by darker shades to the right. Note the bimodal distribution for DA with some being very close to 0, which indicates isotropic organization. This distribution and range is the cause for the large standard deviations found in Table 3.

Figure 5. Metacarpal regional variation for the post-Neolithic and forager samples. Values of BV/TV, E, and DA are mapped onto right hands. The darkened areas in the palmar view represent the respective head/base segments. Here BV/TV and E both show a tendency for the heads to have higher relative values in the palmar/palmar-ulnar Mc2–Mc5 and palmar-radial

Mc1. Also note the variation in DA between the two samples. The data pictured here pertains to model type 2.

Figure 6. Phalangeal regional variation for the post-Neolithic and forager samples. Values of BV/TV, E, and DA are mapped onto rights hands in palmar view. Here there is little variation between the ulnar and radial regions for BV/TV and E, whereas DA varies more. Data pictured here pertains to model type 3.

Figure 7. Palmar (A) and dorsal (B) views of the average site-specific BV/TV for the post-Neolithic and forager samples. While both distributions are generally similar in the high value concentrations along the metacarpal and phalangeal head/ bases, the values for the forager sample are generally higher with the carpals and phalangeal heads being the most different.

Figure 8. Distal (A) and proximal (B) views of the average metacarpal site-specific BV/TV for the post-Neolithic and forager samples. Note how the relatively high site-specific BV/TV values in the palmoulnar Mc2–Mc5 heads and palmoradial Mc1 heads match the metacarpal regional variation for BV/TV and E (Fig. 5).

Figure 9. Proximal (A) and distal-palmar (B) view of average carpal site-specific BV/TV for the post-Neolithic and forager samples. Note the differences in high values concentrations along the radial surface of the triquetral, radiocarpal (proximal lunate and scaphoid), and midcarpal joints (distal lunate and scaphoid).

Figure 10. Ulnar-proximal (A) and radial-proximal (B) views of average hamate, capitate, and trapezoid site-specific BV/TV for the post-Neolithic and forager samples. Here both samples show high value concentrations along the capitate that correspond with those observed on the

lunate and scaphoid. Also note the correspondence of high value concentrations between the forager trapezoid and capitate that are not present in the post-Neolithic sample (B).

Figure 11. Cross-sectional views through the lunate, capitate, and ray III for post-Neolithic males with relatively low (A) and high (B) site-specific BV/TV throughout the hand. Note the similar distributions of relatively high BV/TV values at the dorsal aspect of the lunate, capitate head, palmar metacarpophalangeal joint, and dorsal interphalangeal joint.

Figure 1.

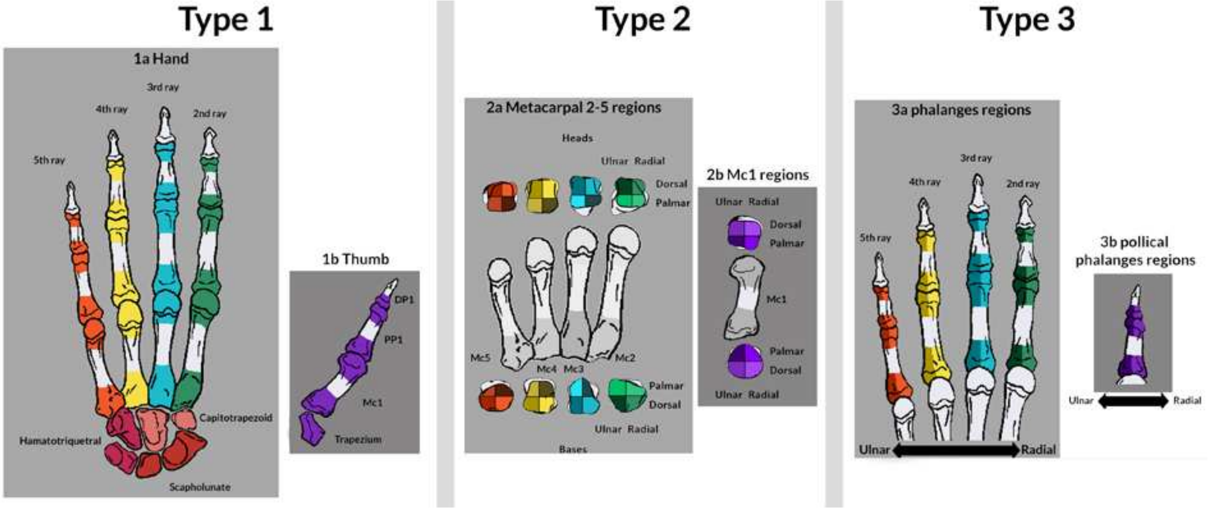
Type 1
1a Hand
3rd ray
4th ray
2nd ray
5th ray
Capitotrapezoid
Hamatotriquetral
Scapholunate
1b Thumb
DP1
PP1
Mc1
Trapezium
Type 2
2a Metacarpal 2-5 regions
Heads
Ulnar Radial
Dorsal
Palmar
Mc5
Mc4 Mc3
Mc2
Palmar
Dorsal
Ulnar Radial
Bases
2b Mc1 regions
Ulnar Radial
Dorsal
Palmar
Mc1
Palmar
Dorsal
Ulnar Radial
Type 3
3a phalanges regions
3rd ray
4th ray
2nd ray
5th ray
Ulnar
Radial
3b pollical phalanges regions
Ulnar
Radial

Figure 2.

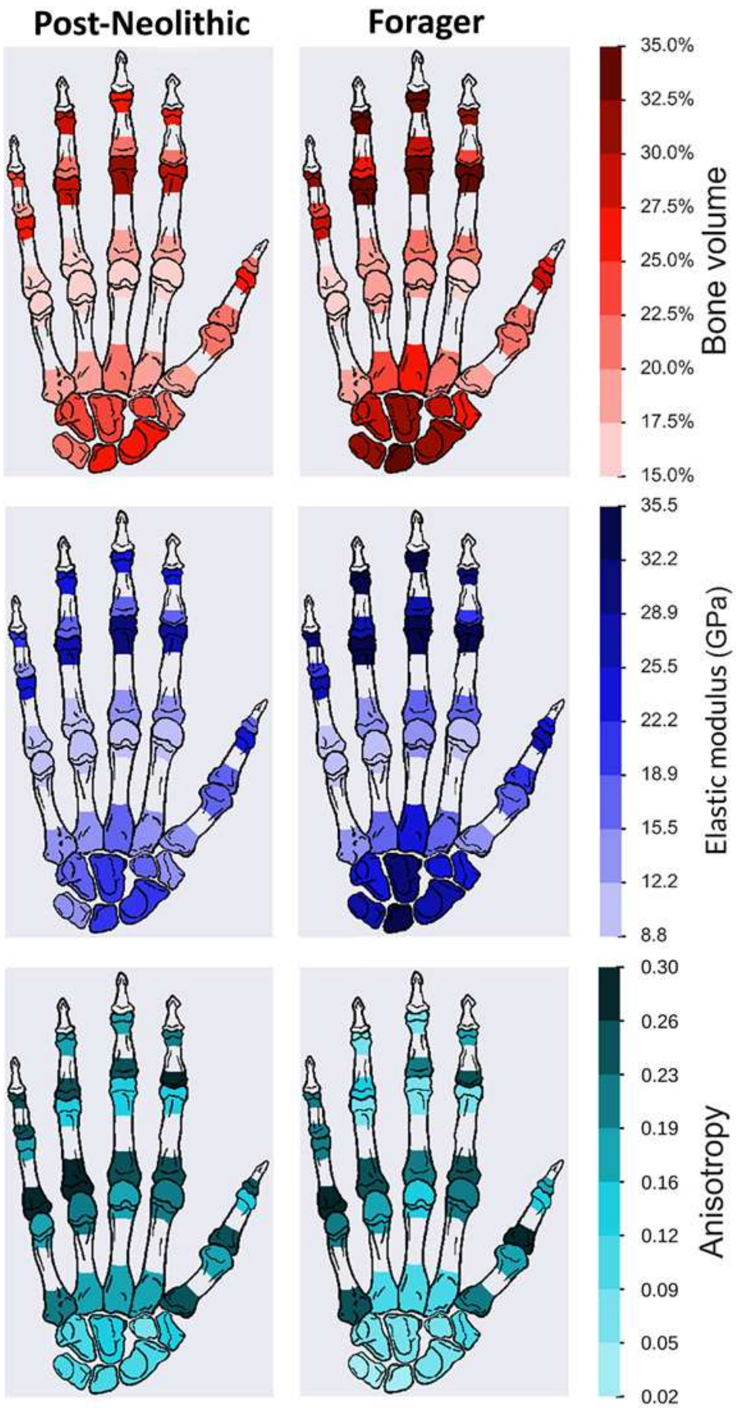
Post-Neolithic
Forager
35.0%
32.5%
30.0%
27.5%
25.0%
22.5%
20.0%
17.5%
15.0%
Bone volume
35.5
32.2
28.9
25.5
22.2
18.9
15.5
12.2
8.8
Elastic modulus (GPa)
0.30
0.26
0.23
0.19
0.16
0.12
0.09
0.05
0.02
Anisotropy

Figure 3.

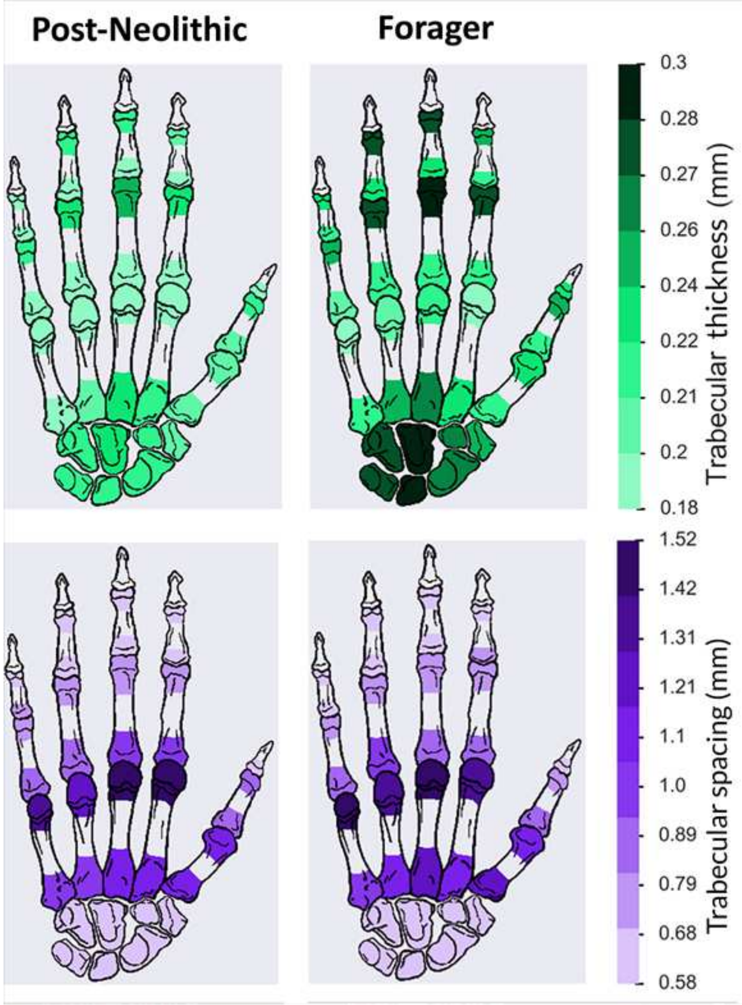
Post-Neolithic
Forager
0.3
0.28
0.27
0.26
0.24
0.22
0.21
0.2
0.18
Trabecular thickness (mm)
1.52
1.42
1.31
1.21
1.1
1.0
0.89
0.79
0.68
0.58
Trabecular spacing (mm)

Figure 4.

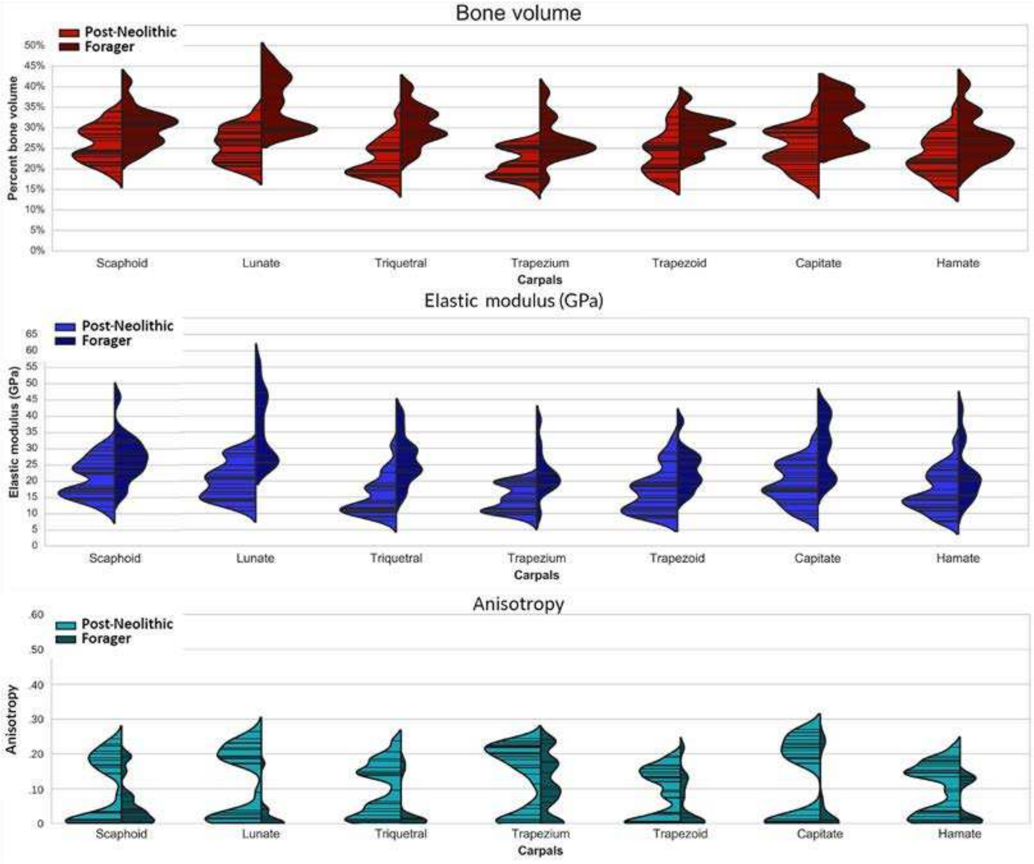
Bone volume
Post-Neolithic
Forager
Percent bone volume
0%
5%
10%
15%
20%
25%
30%
35%
40%
45%
50%
Scaphoid
Lunate
Triquetral
Trapezium
Trapezoid
Capitate
Hamate
Carpals
Elastic modulus (GPa)
Post-Neolithic
Forager
Elastic modulus (GPa)
0
5
10
15
20
25
30
35
40
45
50
55
60
65
Scaphoid
Lunate
Triquetral
Trapezium
Trapezoid
Capitate
Hamate
Carpals
Anisotropy
Post-Neolithic
Forager
Anisotropy
0
.10
.20
.30
.40
.50
.60
Scaphoid
Lunate
Triquetral
Trapezium
Trapezoid
Capitate
Hamate
Carpals

Figure 5.

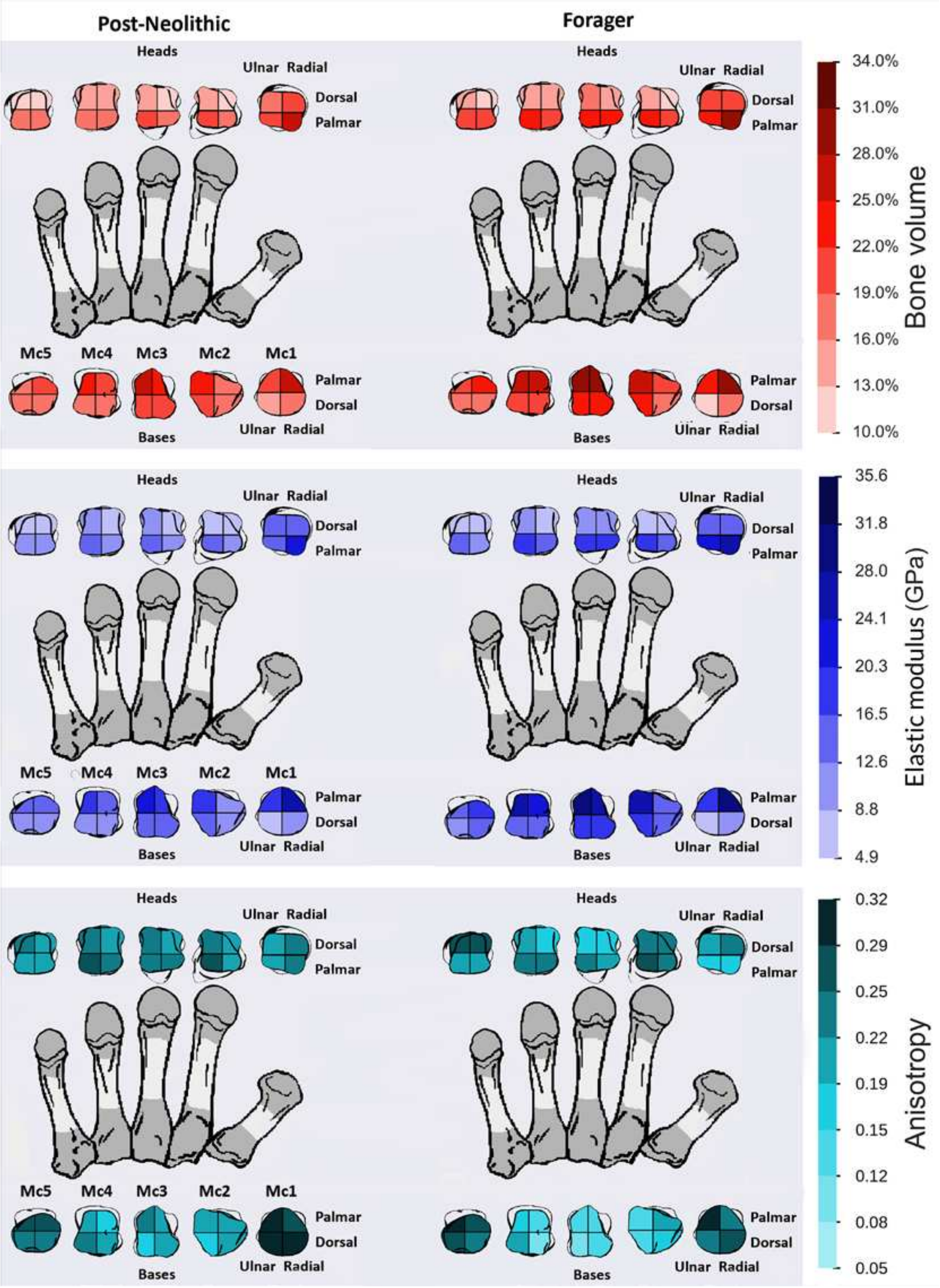
Post-Neolithic
Forager
Heads
Ulnar Radial
Dorsal
Palmar
Mc5
Mc4
Mc3
Mc2
Mc1
Palmar
Dorsal
Bases
Ulnar Radial
Bone volume
34.0%
31.0%
28.0%
25.0%
22.0%
19.0%
16.0%
13.0%
10.0%
Elastic modulus (GPa)
35.6
31.8
28.0
24.1
20.3
16.5
12.6
8.8
4.9
Anisotropy
0.32
0.29
0.25
0.22
0.19
0.15
0.12
0.08
0.05

Figure 6.

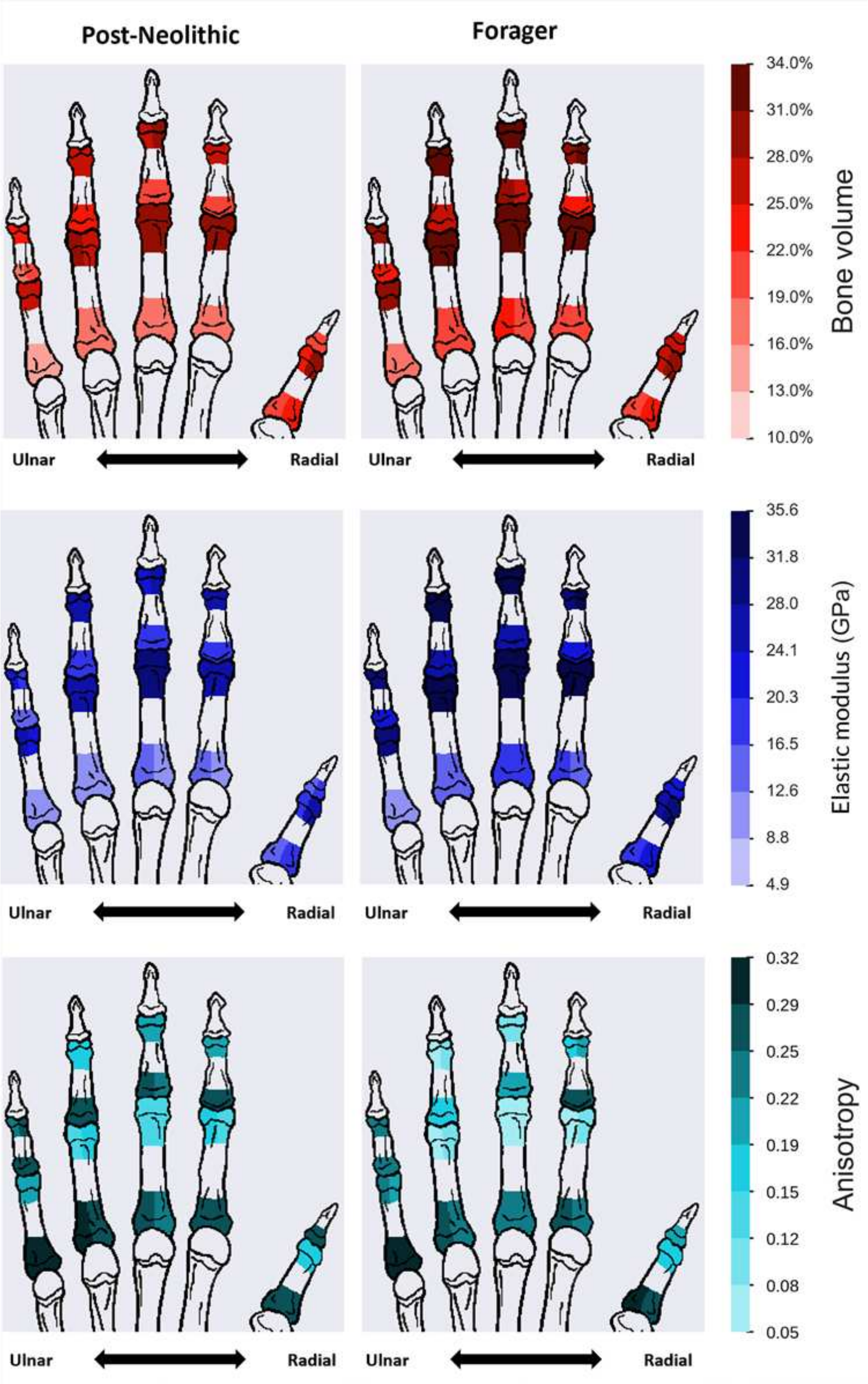
Post-Neolithic
Forager
34.0%
31.0%
28.0%
25.0%
22.0%
19.0%
16.0%
13.0%
10.0%
Bone volume
Ulnar
Radial
Ulnar
Radial
35.6
31.8
28.0
24.1
20.3
16.5
12.6
8.8
4.9
Elastic modulus (GPa)
Ulnar
Radial
Ulnar
Radial
0.32
0.29
0.25
0.22
0.19
0.15
0.12
0.08
0.05
Anisotropy
Ulnar
Radial
Ulnar
Radial

Figure 7.

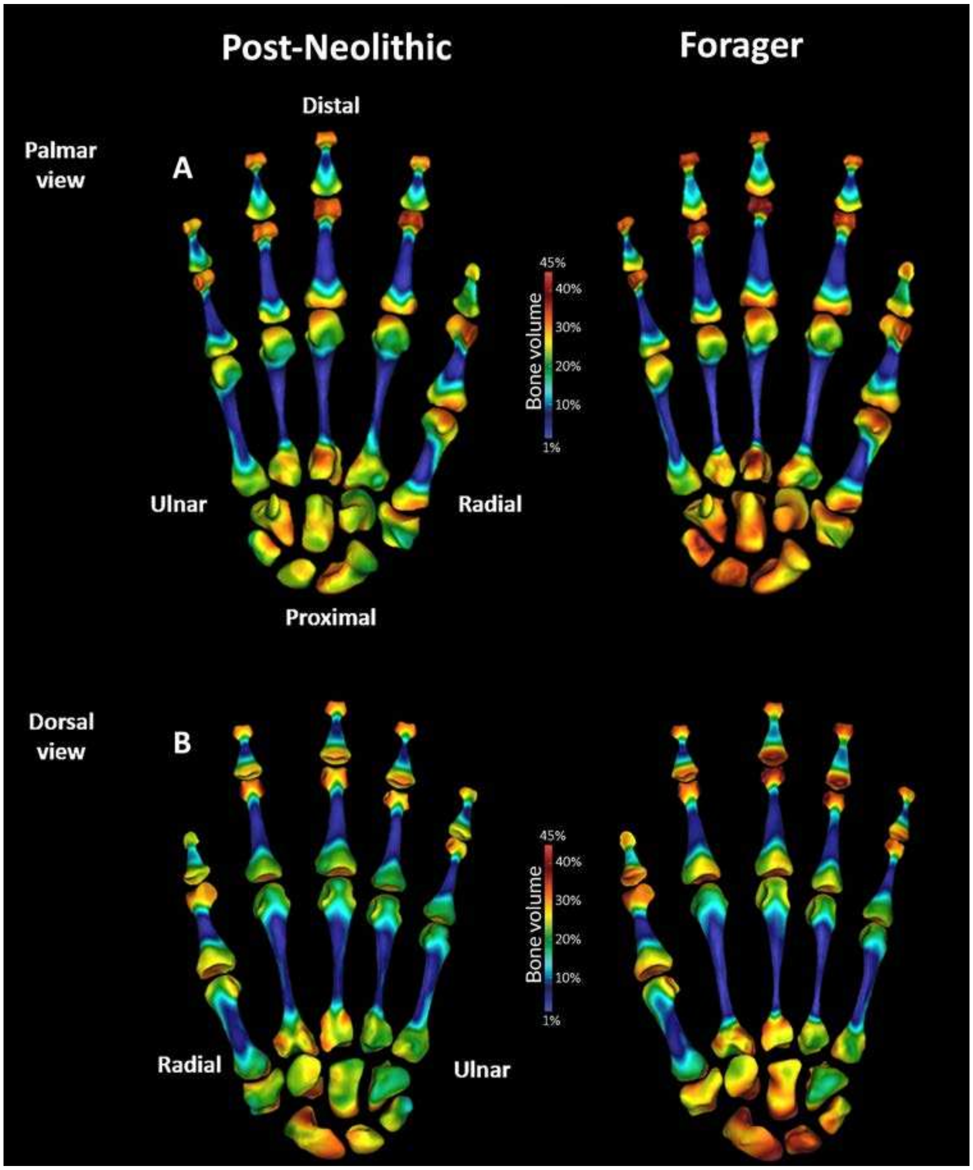
Post-Neolithic
Forager
Distal
Palmar view
A
Ulnar
Radial
Proximal
45%
40%
30%
20%
10%
1%
Bone volume
Dorsal view
B
Radial
Ulnar
45%
40%
30%
20%
10%
1%
Bone volume

Figure 8.

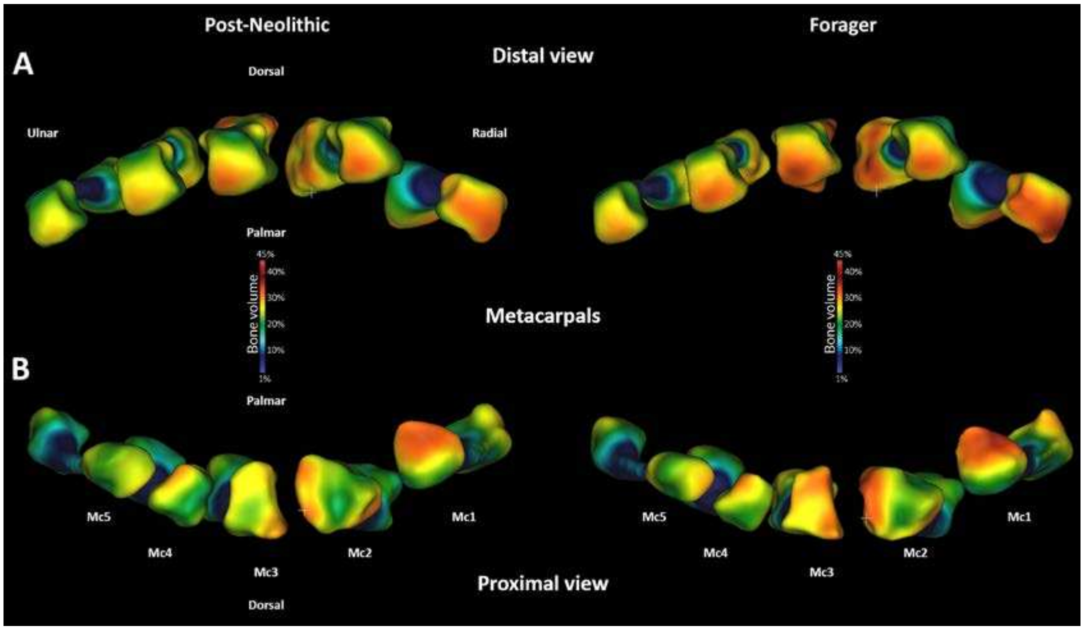
Post-Neolithic
Forager
A
Distal view
Dorsal
Ulnar
Radial
Palmar
45%
40%
30%
20%
10%
1%
Bone volume
Metacarpals
B
Palmar
Mc5
Mc4
Mc3
Mc2
Mc1
Proximal view
Dorsal

Figure 9.

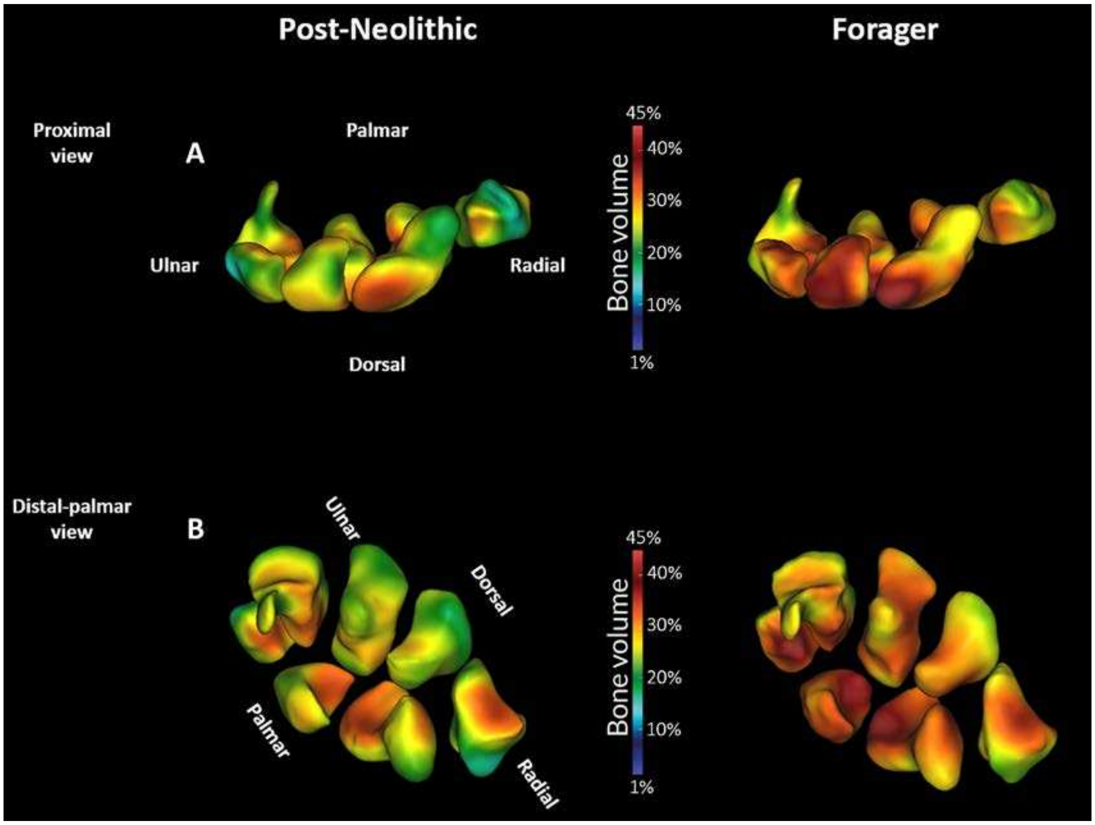
Post-Neolithic
Forager
Proximal view
A
Palmar
Ulnar
Radial
Dorsal
45%
40%
30%
20%
10%
1%
Bone volume
Distal-palmar view
B
Ulnar
Dorsal
Palmar
Radial
45%
40%
30%
20%
10%
1%
Bone volume

Figure 10.

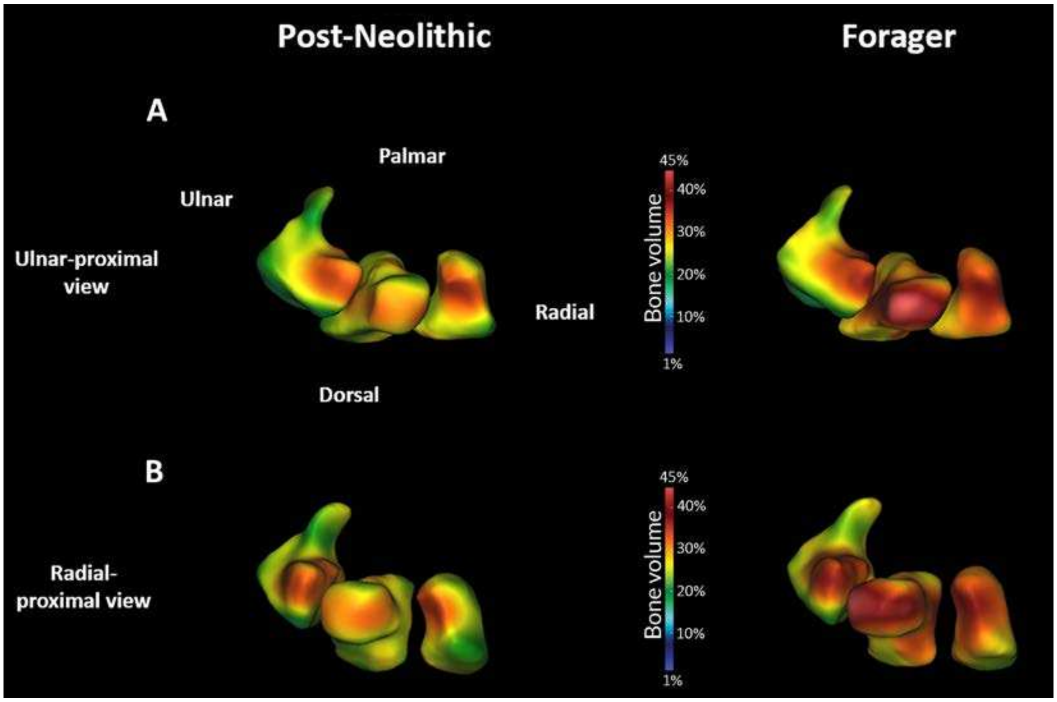
Post-Neolithic
Forager
A
Palmar
Ulnar
Ulnar-proximal view
Radial
Dorsal
Bone volume
45%
40%
30%
20%
10%
1%
B
Radial-proximal view
Bone volume
45%
40%
30%
20%
10%
1%

Figure 11.

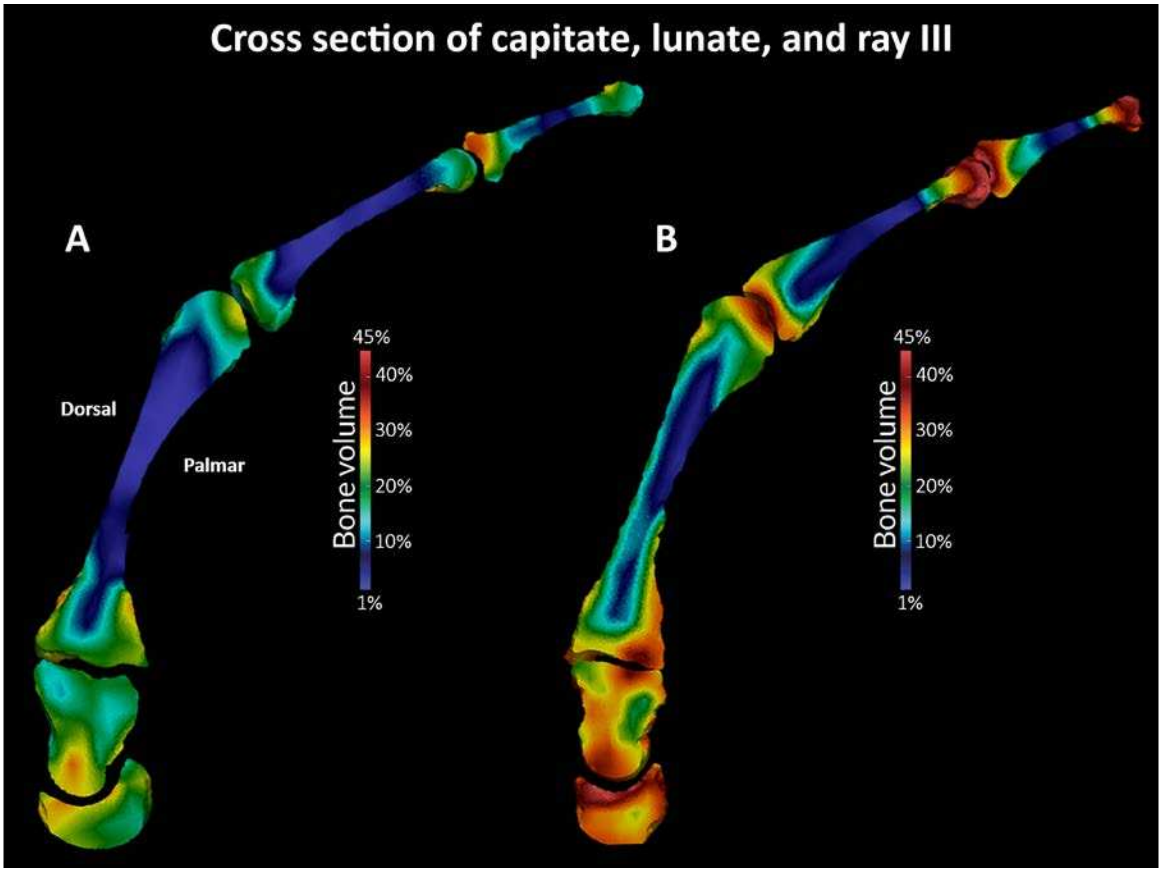
Cross section of capitate, lunate, and ray III
A
Dorsal
Palmar
45%
40%
30%
20%
10%
1%
Bone volume
B
45%
40%
30%
20%
10%
1%
Bone volume

Table 1

Summary of manual elements per group.

Carpal	Total	PN	For.	Mc	Total	PN	For.	PP	Total	PN	For.	IP and DP	Total	PN	For.
Capitate	40	30	10	First	51	32	19	First	38	25	13	Distal first	39	27	12
Hamate	42	30	12	Second	55	32	23	Second	32	17	15	Second	37	24	13
Lunate	38	27	11	Third	55	33	22	Third	45	29	16	Third	44	31	13
Scaphoid	46	29	17	Fourth	47	33	14	Fourth	46	30	16	Fourth	37	24	13
Trapezium	41	29	12	Fifth	40	31	9	Fifth	42	29	13	Fifth	26	18	8
Trapezoid	43	30	13												
Triquetral	35	24	11												

Abbreviations: DP = distal phalanx; For. = number of bones in forager sample; IP = intermediate phalanx; Mc = metacarpal; PN = number of bones in post-Neolithic sample; PP = proximal phalanx; Total = combined number of bones within the sample.

Table 2

Summary of terms used within the linear mixed effect models and their predictions.[a]

Term	Definition
Sample	Post-Neolithic or forager
Skeletal element	The osteological designation of each bone (i.e., capitate, first metacarpal, etc.)
Segment	Unit of skeletal element analyzed. Specifically, whole carpal or subdivided region of a metacarpal/phalanx (i.e., carpal, base, or head)
Region	Subdivided metacarpal/phalangeal head or base segment:
	Metacarpal: dorsoradial, dorsoulnar, palmoradial, palmoulnar
	Phalanx: radial and ulnar
Region group	Used to group together the region measurements belonging to the same head or base: specimen + side + skeletal element + segment
Side	Side of the body a bone is from (i.e., right or left)
Specimen	Accession or individual identification (e.g., Qafzeh 8)
Hand ID	Identifier to distinguish the right and left hands of the same individual: side + specimen
Specific ID	Unique identifier used to prevent repeated analysis of a bone (pseudoreplication): Defined as skeletal element + specimen + side
Functional group	A grouping of functionally related skeletal elements and their respective segments/regions:
	Scapholunate: Scaphoid and lunate
	Capitotrapezoid: Trapezoid and capitate

	Hamatotrqiuetral:	Hamate and triquetral
	Thumb:	Trapezium, Mc1, first intermediate phalanx and the distal phalanx
	Ray II:	Mc2, and the second proximal and intermediate phalanx
	Ray III:	Mc3, and the third proximal and intermediate phalanx
	Ray IV:	Mc4, and the fourth proximal and intermediate phalanx
	Ray V:	Mc5, and the fifth proximal and intermediate phalanx
Model type 1	Contains data from carpals, thumb, and rays II-V head/base segments:	
Prediction	Similar distribution patterns for both samples, but the forager values will be significantly higher for BV/TV, E, and lower for DA.	
Model type 2	Contains data from Mc1-Mc5 head/base regions:	
Prediction	BV/TV and E distribution will reflect flexion and adduction/abduction, but the foragers' values will be significantly higher.	
Model type 3	Contains data from PP1-PP5 head/base, IP2-IP5 head/base, and DP1 base regions:	
Prediction	BV/TV and E distribution will reflect flexion at the interphalangeal joints, but the foragers' values will be significantly higher.	

Abbreviations: DP = distal phalanx; IP = intermediate phalanx; Mc = metacarpal; PP = proximal phalanx.

[a] Note that the functional groups for each model contain only the relevant segments and or regions (e.g., metacarpal regions are excluded from models testing only the differences between phalanges). See SOM S2 for a detailed description of each functional group. Note that the predictions for DA are not included because the models were rejected (see SOM S3 for details).

1833